565 (1970). [This updates Los Alamos Scientific Laboratory Report No. LA-3753 (1967).]
[12]D. T. Cromer and J. B. Mann, Acta Cryst. A24, 321 (1968).
[13]H. P. Hanson, F. Herman, J. D. Lea, and S. Skillman, Acta Cryst. 17, 1040 (1964).
[14]J. C. Slater, Phys. Rev. 81, 385 (1951).
[15]W. Heisenberg, Z. Physik 32, 737 (1931).
[16]L. B. Mendelsohn and F. Biggs, Phys. Rev. A 5, 688 (1972).
[17]D. T. Cromer and J. B. Mann, J. Chem. Phys. 47, 1892 (1967).
[18]R. F. Pohler and H. P. Hanson, J. Chem. Phys. 42, 2347 (1965).
[19]D. E. Parks and M. Rotenberg, Phys. Rev. A 5, 521 (1972).

PHYSICAL REVIEW A VOLUME 7, NUMBER 3 MARCH 1973

Universal Cross Sections for K-Shell Ionization by Heavy Charged Particles. I. Low Particle Velocities*

George Basbas,† Werner Brandt, and Roman Laubert
Department of Physics, New York University, New York, New York 10003
(Received 8 August 1972)

Experimental K-shell ionization cross sections are reported for low-velocity heavy projectiles of atomic number small compared to the target atomic number. For such projectile-target combinations, the Coulomb interaction between the projectile nucleus and the K-shell electrons dominates the K-shell ionization process at all projectile velocities. The data can disagree by orders of magnitude with the primary predictions of the nonrelativistic quantum theory in the plane-wave Born approximation. Important physical processes are shown to be at the root of the discrepancies. They derive from the finite charge of the moving projectile, and thus do not contribute in the plane-wave Born approximation. They are the Coulomb deflection of the projectile in the field of the target nucleus and the perturbation of the target atomic states by the projectile. A theory for these processes is developed in an approximate manner. When incorporated with the theory in the plane-wave Born approximation, it accounts quantitatively for the data. A method results for reducing cross-section data in a comprehensive way. A universal graph of cross sections emerges which, in effect, constitutes an extrapolation of the data to the conditions of zero projectile charge. It comprises cross sections ranging over six orders of magnitude measured on different targets for various projectiles with a wide range of velocities, mostly below the mean K-shell velocities. The locus of this universal graph coincides with the prediction of the plane-wave Born approximation.

I. INTRODUCTION

This is the first of two papers on K-shell ionization of atoms in collision with atomic projectiles. We report measurements of cross sections for such events and present a comprehensive comparison of existing data with theory. New effects appear. Their interpretation gives fresh insight into the dynamics governing inner-shell excitations.

The distinction between projectile and target is not linked to the preparation of the projectile beam before entering the target. Both can be ionized and both will fill their own K-shell vacancy with the emission of an Auger electron or a characteristic x ray. The x ray counted in the laboratory determines the target. In the following this is in fact always the laboratory target. The projectiles, with properties marked by the subscript 1, impinge upon stationary target atoms with properties marked by the subscript 2.

In considering the wide range of possible projectile-target combinations, the subject of K-shell ionization divides itself into well-circumscribed domains. We distinguish between projectiles that act as bare point-charge particles in the encounter leading to K-shell ionization, and those that do not. And we set apart slow and fast collisions relative to the response time of the K-shell electrons to be excited.

Projectiles that act as mass points of charge Z_1e when exciting target K-shell electrons are referred to as charged particles. Target K-shell electrons are excited by charged particles only via the Coulomb interaction between the projectile nucleus and the target electrons and, hence, cause *Coulomb excitation* of K shells. Coulomb excitation always dominates at projectile velocities so high that the projectiles move as bare nuclei through the target. But even a slow projectile carrying an electronic structure acts as a bare charged particle provided that its K-shell radius a_{1K} is large compared to the target K-shell radius a_{2K}. This is because at low projectile velocities K-shell ionization occurs only on deep penetration by the particle to internuclear distances much less than a_{2K}.[1] Thus, the projectile electrons will be found mainly outside the interaction region, leaving the projectile nucleus to excite the target

K shell as a bare charged particle.

The condition $a_{1K} \gg a_{2K}$ imposes the condition $Z_1 \ll Z_2$ on the nuclear charge since $a_{1K} = a_0/Z_{1K}$ and $a_{2K} = a_0/Z_{2K}$, where a_0 denotes the Bohr radius and $Z_{1K}e = e$ for $Z_1 = 1$, $Z_{1K}e = (Z_1 - 0.3)e$ for $Z_1 > 1$, and $Z_{2K}e = (Z_2 - 0.3)e$ denote the screened nuclear charges. The condition of deep penetration follows from the circumstance that the impact parameters which contribute most to ionization[1] have values $\simeq q_0^{-1}$, where $\hbar q_0 = \hbar\omega_{2K}/v_1$ denotes the minimum momentum transfer in the ionization of a K-shell electron with binding energy $\hbar\omega_{2K}$ by a heavy projectile of mass M_1 and energy $E_1 = \frac{1}{2}M_1 v_1^2$ much larger than $\hbar\omega_{2K}$. Therefore, slow projectiles, for which $q_0^{-1} \ll a_{2K}$, must penetrate deeply into the K shell to remove a K-shell electron. In the following we usually express $\hbar\omega_{2K}$ in terms of the dimensionless parameter $\theta_K \equiv \hbar\omega_{2K}/Z_{2K}^2\mathcal{R}$ which measures the nonhydrogenic aspect of the K-shell ionization energy ($\mathcal{R} = \frac{1}{2}$ a.u. $= 13.6$ eV); it grows slowly with Z_2 from $\simeq 0.6$ for light elements to $\simeq 0.9$ for heavy elements. Denoting the mean K-shell velocity as $v_{2K} = Z_{2K}v_0$ (v_0 is the Bohr velocity), the condition $q_0^{-1} \ll a_{2K}$ implies $v_1 \ll \omega_{2K}a_{2K} = \frac{1}{2}\theta_K v_{2K}$.

Thus, when $Z_1 \ll Z_2$, all projectiles act as bare point charges at velocities $v_1 \ll \frac{1}{2}\theta_K v_{2K}$. At higher velocities stripping of the projectile K shell can take place; when stripping occurs, the projectile again acts as a bare point charge.

Slow projectiles with $Z_1 \gtrsim Z_2$ carry their electron clouds into the ionizing encounter inside the target K shell and thus act as *ions* or *atoms* and not as point-charge particles. They excite the target K shell through the exchange forces set up by the Pauli exclusion principle in the overlapping electron clouds, as well as by Coulomb excitation. For example, the electrons can respond by following diabatically the transient quasimolecular orbitals leading to electron promotion which makes enhanced excitation possible. We generically characterize these excitation processes as being caused by *Pauli excitation* of atoms in collision. At low velocities, $v_1 \ll v_{2K}$, Pauli excitation overshadows Coulomb excitation. At higher velocities, $v_1 \gtrsim (v_{1K}$ or $v_{2K})$, the response time of the bound electrons is too long compared to the collision time to allow the Pauli principle to influence the ionization process, and Coulomb excitation dominates once more.

Coulomb excitation and Pauli excitation differ in basic ways. They can give rise to widely different K-shell ionization cross sections. Our two papers limit the discussion to projectile-target combinations with $Z_1 \ll Z_2$ and thus are concerned only with Coulomb excitation of K-shell electrons by heavy charged particles. The adjective heavy, here meaning relative to the electron mass, will usually be omitted in the following. In the experiments to be discussed, the heavy charged particles are in fact mostly light nuclei, such as H^+, D^+, He^{++}, and Li^{3+}, impinging on targets for which Coulomb excitation dominates. Projectiles with $Z_1 \simeq Z_2$ and the relative importance of Coulomb and Pauli excitation will be covered elsewhere.

A meaningful and convenient demarcation between slow and fast collisions is set by the time it takes for the projectile to traverse the target K shell, $\simeq a_{2K}/v_1$, compared to the characteristic time of the target K-shell electron ω_{2K}^{-1}. The condition $a_{2K}/v_1 \gg \omega_{2K}^{-1}$, identifying slow collisions and hence low velocities, is just the condition $q_0^{-1} \ll a_{2K}$ which requires deep penetration for ionization to occur at low velocities. This condition obtains when the central parameter

$$\xi_K \equiv (q_0 a_{2K})^{-1} = v_1/\tfrac{1}{2}\theta_K v_{2K} \tag{1}$$

has values $\ll 1$. Fast collisions or high-velocity conditions prevail when $\xi_K \gg 1$.

It is customary to express the projectile-velocity dependence of the cross sections through the reduced particle-velocity parameter:

$$\eta_K \equiv v_1^2/v_{2K}^2 = v_1^2/v_0^2 Z_{2K}^2 = (\theta_K/2)^2\xi_K^2, \tag{2}$$

which is proportional to the projectile energy. Note that $\eta_K \simeq 40E_1$ (in MeV)$/Z_{2K}^2 M_1$ (in amu). The demarcation $\xi_K \simeq 1$ separates the domains of low velocities and of high velocities. In the high-velocity domain, to be discussed in Paper II, the particles have energies higher than $\simeq 0.5$ MeV/amu in light targets and higher than $\simeq 50$ MeV/amu in heavy targets.

That heavy charged particles, so slow that $v_1 \ll v_{2K}$, nevertheless do produce inner-shell ionizations has held the interest of physicists for many years. The holes or vacancies created in the process are filled by electrons with the emission of characteristic x rays or of Auger electrons usually after time periods long compared to the collision time. Characteristic x rays emitted under particle bombardment were observed first by Chadwick[2] just 60 years ago. The tight binding of the electrons to the target nucleus, as first argued by Gerthsen,[3] is the crux for an understanding of the characteristic x-ray production by slow heavy particles. The general theory for K-shell ionization by Coulomb excitation has been developed for some time.[1,4] A detailed test of the theory became possible only very recently with the accumulation of wide-ranging accurate cross-section measurements.[5–13]

The classical binary-collision theory was applied recently to this problem.[14] Its predictions differ in some respects from those of the quantum-mechanical[4] and semiclassical formulations.[1] The disparities cannot be resolved by experimental tests, of course. They must await clarification on theoretical grounds.

This paper presents new material and incorporates data, methods, and ideas that have accrued over the

past several years.[6–8,10,12,13] A concise summary was given recently.[15] Section II reports new data. Inspection of the measurements to date reveals, in Sec. IV, that the K-shell ionization cross sections in the low-velocity domain are grossly at variance with some of the primary predictions of the quantum theory of K-shell ionization cross sections in the only fully developed approximation which is the plane-wave Born approximation (PWBA) summarized in Sec. III. Certain key features of the PWBA are identified as being at the root of the discrepancies between theory and experiment. Methods of improving upon the theory are given in Sec. V. Finally, in Sec. VI, our new theoretical predictions are tested by a comprehensive comparison with experiments. A universal graph of K-shell ionization cross sections issues from this comparison. It extends over six orders of magnitude and comprises data for several different charged particles, with velocities ranging over two orders of magnitude in η_K, incident on targets of atomic numbers between 6 and 29.

II. NEW DATA

Our previous measurements[8] of characteristic x-ray production yields were limited to ions of $^1_1$H, $^3_2$He, and $^4_2$He on aluminum in the energy range 20–200 keV, restricting the range of ξ_K [Eq. (1)] to values below unity. In this section we report data for these particles up to 3 MeV, extending the range to just beyond $\xi_K = 1$. This permits us, at least for Al, to test the theory over the entire low particle-velocity domain.

A. Experimental Arrangements

The apparatus is similar to that described elsewhere.[8] With the use of the van de Graaff accelerator at the Department of Terrestrial Magnetism of the Carnegie Institution of Washington, we could extend the particle-energy range to 3 MeV/amu. The beam, defined by projectile energy and mass in a 7° analyzing magnet, impinged on a target of high-purity (99.999%) aluminum foil inclined 45° with respect to the beam direction and to the line of sight of the photon detector. The foil was thick enough, 2.5×10^{-2} cm, to stop the particles at all energies and thus produced "thick-target x-ray yields." The target, heated to 150 °C to suppress carbon deposition, was electrically biased to ensure a proper current measurement.[7] A 4-in. oil diffusion pump with a molecular sieve maintained a pressure in the target chamber of less than 5×10^{-5} Torr under all operating conditions. Visual inspection of the target after bombardment showed no evidence of carbon deposition. A flow-mode proportional counter connected to a multichannel analyzer recorded the x rays emitted from the target. Aluminum absorbers between the target and the counter prevented scattered particles from entering the counter. The total x-ray yield is obtained by an appropriate integration over the x-ray energy spectrum as recorded for preset values of the integrated beam current.

Several strong Al (p,γ)Si resonance reactions occur in the energy range of this experiment. To ensure that the resulting γ rays do not contribute measurably to the total x-ray yield, measurements were made at and just below the resonance energies. No significant change was observed in the total x-ray yield.

To connect the present experiments to our low-energy measurements[8] a molecular hydrogen-ion beam was extracted from the van de Graaff accelerator. Also, the earlier measurements were extended at the New York University accelerator from 200 to 300 keV to provide a broad region of energy overlap between the two sets of data. We illustrate the consistency of the data collected for protons and H_2^+ incident on aluminum in Fig. 1. Each data point represents an average of three to five measurements. The data measured with the molecular

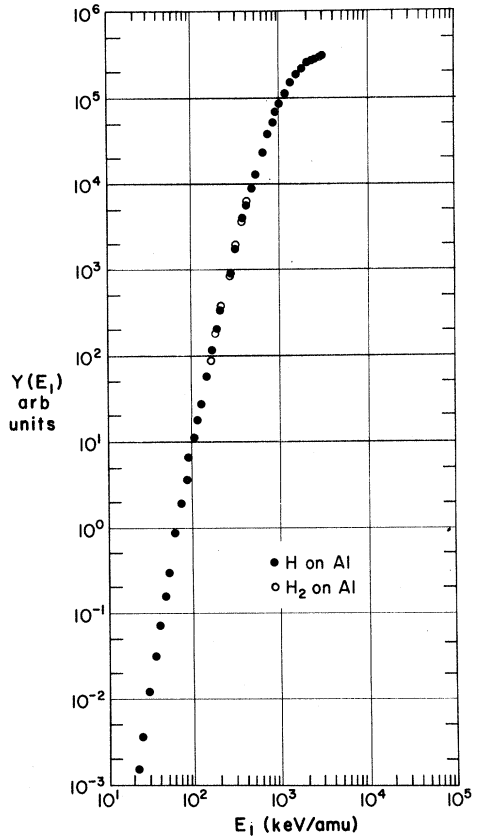

FIG. 1. Thick-target yields of Al(K) characteristic x rays produced by protons as a function of the incident energy E_1. The experimental uncertainties are comparable to the size of the dots.

hydrogen-ion beam agree with the proton induced x-ray yields. To maintain the proportional counter in the same range of sensitivity despite the vast range of yields under investigation, we changed the detector acceptance angle and inserted aluminum absorbers between the target and the counter. Whenever this was done, a series of at least ten yield measurements determined the combined angle and filter diminution factor.

The $^3_2$He and $^4_2$He data were normalized to the proton results by introducing $^1_1H_2$-$^4_2$He and $^3_2$He-$^4_2$He gas mixtures into the ion source and measuring, within minutes of each other, the respective thick-target x-ray yields of the $^1_1H^+$ and $^4_2He^+$ beams resulting from the former and the $^3_2He^+$ and $^4_2He^+$ beam from the latter mixture. The data for $^4_2$He with incident energies above 3 MeV were obtained with a $^4_2He^{2+}$ beam. The rf ion source employed on this occasion was fed with helium gas exclusively; this minimized the possibility of contamination of $^4_2He^{2+}$ beam with $^1_1H_2^+$ beam. Thick-target x-ray yield measurements between 2 and 3 MeV with singly and doubly charged helium agreed within the experimental error.

The data for the aluminum K-shell x-ray yield under deuterium bombardment were collected at the New York University heavy-ion accelerator facility.[16] Since the analyzing magnets cannot separate deuterium ions from H_2^+ ions of the same energy, precautions had to be taken to avoid beam contamination. The reported results were obtained with a pure beam in the sense that atomic and molecular deuterium beams at the same energy/amu gave identical x-ray yields.

B. Data Analysis and Results

Our experiments measure the number of characteristic Al (K) photons emitted in the wake of the K-shell ionizations generated by incident particles of initial energy E_1. To the extent that the x rays are emitted isotropically,[17] the x-ray production cross section $\sigma_x(E_1)$ can be determined from the formula

$$\sigma_x(E_1)=\frac{4\pi}{n\Omega\gamma}\left[\left(\frac{dY(E_1')}{dE_1'}\,\frac{dE_1'}{dR_p(E_1')}\right)_{E_1'=E_1}+\mu\,\frac{\cos\vartheta}{\cos\varphi}\;Y(E_1)\right], \tag{3}$$

where n is the number density of the target atoms, Ω and γ are the acceptance angle and the efficiency of the detector, respectively, and $Y(E_1)$ is the average number of characteristic x rays registered by the detector per incident particle. The best curve through the values of $Y(E_1)$ forms the experimental x-ray excitation function, with the slope $dY(E_1')/dE_1'$ evaluated at $E_1'=E_1$. The projected range of the bombarding particle along the direction of the incident beam is $R_p(E_1')$ and μ is the absorption coefficient of the target for its own characteristic x rays. The angles ϑ and φ are formed, respectively, by the beam direction and by the line of sight from the beam spot to the detector with respect to the normal of the target surface at the point of beam impact. The function

$$\frac{dE_1}{dR_p}=S(E_1)\left(\frac{dR(E_1')}{dR_p(E_1')}\right)_{E_1'=E_1} \tag{4}$$

depends on the stopping power of the material for the incident ions $S(E_1)$ and on the detour factor $[dR(E_1')/dR_p(E_1')]_{E_1'=E_1}$, which measures the deviation of the range of the particle from its projection along the incident beam direction. The detour factor for the ion-target systems under study differs from unity by 1% or less.

In our experiment $\vartheta=\varphi=45°$, and Eq. (3) simplifies to

$$\sigma_x(E_1)=\frac{4\pi}{n\Omega\gamma}\left[S(E_1)\left(\frac{dY(E_1')}{dE_1'}\right)_{E_1'=E_1}+\mu\;Y(E_1)\right]. \tag{5}$$

For definiteness, the product of the solid angle and the efficiency of the counter $\Omega\gamma$ is calibrated by equating our thick-target Al (K) x-ray yield for incident protons at $E_1=100$ keV to the yield of 1.61×10^{-6} x rays/proton measured by Khan *et al.*[5] Should this reference value need revision in the future, all our cross sections can be readjusted through multiplication by a constant factor.

The largest source of error encountered in the determination of the x-ray production cross section at low projectile energies, where transmission experiments are not feasible and differential yields must be determined from the thick-target yields, derives from the calculation of the slope of Y with regard to E_1. We have explored sophisticated procedures on the CDC 6600 computer to fit different types of functions[18] to $Y(E_1)$ which could then be differentiated analytically. It is difficult to decide which procedure and function give best slopes since all these slope values and those derived by graphical methods agree to within 10–20% over the entire energy range. We conclude on the basis of this study that an adequate fit to $Y(E_1)$ can be accomplished by a 3- to 7-order polynomial with the aid of a programmable electronic desk calculator such as the Wang 700. The yield values obtained from the fit are denoted $Y_f(E_i)$.

Tables I–IV list the measured Al (K) thick-target yields $Y(E_1)$, the fitted yields $Y_f(E_1)$, and the slopes $dY_f(E_1)/dE_1$ as needed in Eq. (3) or (5). No $Y_f(E_1)$ value differs by more than 10% from the corresponding experimental value $Y(E_1)$. The root-mean-square deviation of the fitted yields from the experimental values is always less than 4%. The yield values and their derivatives reported in the tables include the factors $4\pi/\Omega\gamma$ [cf. Eq. (5)].

The stopping power enters directly in the determination of the x-ray production cross section from thick-target yields by Eq. (5). No single set of experimental stopping power measurements covers

our wide range of energies which straddles the stopping power maxima. The stopping powers reported in the literature can differ by as much as 20%. We balance the available data by an averaging procedure suggested by Varelas and Biersack.[19] One interpolates through the stopping-power maxi-

TABLE I. Aluminum K-shell x-ray production cross sections $\sigma_x(E_1)$ for incident protons of energies E_1. Column 2 is the measured thick-target x-ray yield $Y(E_1)$ and fitted yield $Y_f(E_1)$ in x rays per incident particle; $Y(E_1)$ is normalized to the result of Khan *et al.* (Ref. 5) of 1.61×10^{-6} x rays/proton obtained for 100-keV incident protons. Column 3 is the slope of the excitation function. Column 4 is the stopping power of aluminum for protons. Column 5 is the x-ray production cross section, in barns, as determined by Eq. (5) with $n=2.23\times10^{19}$ atoms/mg and $\mu=391$ cm^2/g. Numbers in parentheses indicate powers of 10. K-shell ionization cross sections are $\sigma_K^{expt}=\gamma_K^{-1}\sigma_x$.

	Al(K) x-ray yield				
Energy E_1 (MeV) ± 0.5%	$Y(E_1)$	$Y_f(E_1)$ x rays/particle ± 3%	$dY_f(E_1)/dE_1$ x rays/keV particle ± 15%	$S(E_1)$ (keV cm^2/mg) ± 10%	$\sigma_x(E_1)$ (b) ± 25%
2.50(−2)	5.18(−10)	5.00(−10)	1.15(−10)	390	2.02(−3)
3.00(−2)	1.73(− 9)	1.75(− 9)	3.50(−10)	415	6.54(−3)
3.50(−2)	4.60(− 9)	4.80(− 9)	8.20(−10)	435	1.61(−2)
4.00(−2)	1.04(− 8)	1.10(− 8)	1.60(− 9)	452	3.26(−2)
5.00(−2)	4.17(− 8)	4.13(− 8)	5.00(− 9)	472	1.07(−1)
6.00(−2)	1.27(− 7)	1.15(− 7)	1.05(− 8)	478	2.27(−1)
7.00(−2)	2.76(− 7)	2.64(− 7)	2.00(− 8)	478	4.33(−1)
8.00(−2)	5.29(− 7)	5.30(− 7)	3.42(− 8)	472	7.33(−1)
9.00(−2)	9.56(− 7)	9.67(− 7)	5.43(− 8)	463	1.14(0)
1.00(−1)	1.61(− 6)	1.64(− 6)	8.13(− 8)	453	1.68(0)
1.10(−1)	2.53(− 6)	2.62(− 6)	1.16(− 7)	442	2.35(0)
1.20(−1)	3.91(− 6)	3.99(− 6)	1.75(− 7)	432	3.46(0)
1.40(−1)	8.27(− 6)	8.31(− 6)	3.40(− 7)	413	6.44(0)
1.53(−1)	1.22(− 5)	1.23(− 5)	4.00(− 7)	402	7.42(0)
1.60(−1)	1.61(− 5)	1.55(− 5)	5.00(− 7)	395	9.14(0)
1.79(−1)	2.44(− 5)	2.55(− 5)	6.90(− 7)	380	1.22(1)
2.00(−1)	4.83(− 5)	4.26(− 5)	1.05(− 6)	365	1.79(1)
2.04(−1)	4.74(− 5)	4.65(− 5)	1.08(− 6)	363	1.84(1)
2.50(−1)	1.35(− 4)	1.13(− 4)	1.94(− 6)	335	3.11(1)
2.55(−1)	1.29(− 4)	1.23(− 4)	2.05(− 6)	333	3.28(1)
3.06(−1)	2.59(− 4)	2.62(− 4)	3.51(− 6)	310	5.34(1)
3.57(−1)	5.18(− 4)	4.87(− 4)	5.35(− 6)	290	7.81(1)
4.08(−1)	8.63(− 4)	8.14(− 4)	7.51(− 6)	249	9.81(1)
4.59(−1)	1.29(− 3)	1.26(− 3)	9.86(− 6)	263	1.38(2)
5.10(−1)	1.87(− 3)	1.82(− 3)	1.23(− 5)	250	1.70(2)
6.12(−1)	3.23(− 3)	3.33(− 3)	1.72(− 5)	228	2.34(2)
7.14(−1)	5.18(− 3)	5.31(− 3)	2.14(− 5)	210	2.95(2)
8.16(−1)	7.33(− 3)	7.67(− 3)	2.47(− 5)	195	3.50(2)
9.18(−1)	9.92(− 3)	1.03(− 2)	2.68(− 5)	183	4.01(2)
1.02(0)	1.25(− 2)	1.31(− 2)	2.79(− 5)	173	4.46(2)
1.12	1.58(− 2)	1.60(− 2)	2.80(− 5)	162	4.84(2)
1.22	1.75(− 2)	1.89(− 2)	2.74(− 5)	154	5.21(2)
1.33	2.08(− 2)	2.15(− 2)	2.63(− 5)	145	5.48(2)
1.43	2.37(− 2)	2.41(− 2)	2.48(− 5)	138	5.76(2)
1.53	2.59(− 2)	2.66(− 2)	2.31(− 5)	133	6.04(2)
1.63	2.88(− 2)	2.88(− 2)	2.13(− 5)	128	6.27(2)
1.73	3.11(− 2)	3.09(− 2)	1.95(− 5)	124	6.50(2)
1.84	3.31(− 2)	3.28(− 2)	1.78(− 5)	119	6.70(2)
1.94	3.45(− 2)	3.46(− 2)	1.62(− 5)	114	6.89(2)
2.04	3.59(− 2)	3.61(− 2)	1.47(− 5)	110	7.05(2)
2.14	3.74(− 2)	3.76(− 2)	1.34(− 5)	106	7.23(2)
2.24	3.88(− 2)	3.89(− 2)	1.23(− 5)	103	7.39(2)
2.35	4.03(− 2)	4.01(− 2)	1.13(− 5)	100	7.54(2)
2.45	4.14(− 2)	4.12(− 2)	1.05(− 5)	97	7.68(2)
2.55	4.18(− 2)	4.22(− 2)	9.80(− 6)	94	7.81(2)
2.65	4.27(− 2)	4.32(− 2)	9.26(− 6)	92	7.96(2)
2.75	4.34(− 2)	4.41(− 2)	8.87(− 6)	89	8.09(2)
2.85	4.46(− 2)	4.50(− 2)	8.60(− 6)	87	8.23(2)
2.96	4.49(− 2)	4.59(− 2)	8.44(− 6)	85	8.37(2)

mum by taking the sum of the reciprocals of the low- and high-energy stopping powers:

$$[S(E_1)]^{-1} = [S_L(E_1)]^{-1} + [S_B(E_1)]^{-1}, \quad (6)$$

where $S_L(E_1)$ is the low-energy electronic stopping power[20]

$$S_L(E_1) = c_1 \frac{8\pi\, n\, Z_1 Z_2 e^2 a_0}{(Z_1^{2/3} + Z_2^{2/3})^{1/2}} \frac{v_1}{v_0}. \quad (7)$$

The best fit of the factor c_1 to data measured with H and He projectiles is $c_1 \simeq 1.25 Z_1^{1/3}$ rather than the value $c_1 \simeq Z_1^{1/6}$ applicable to heavier projectiles. A modification[19] of the Bethe stopping-power formula

$$S_B(E_1) = C y^{-1} \ln(y + 1 + a/y) \quad (8)$$

is fitted to high-energy stopping-power data, where

$$C = 8\pi\, Z_1^2\, e^4 n / K_B, \quad (9)$$

$$y = 2mv_1^2 / K_B Z_2, \quad (10)$$

and K_B is the Bloch constant.

By adjusting to the standard aluminum value $K_B Z_2 = 163$ eV, we obtain $a = 2.5$ for incident protons and $a = 5$ for helium ions. The stopping power calculated according to Eq. (6) is shown in Fig. 2, with experimental data.[21–28] The electronic stopping powers for $^2_1$D and $^3_2$He are taken to be the same as for $^1_1$H and $^4_2$He, respectively, at the same velocities. The values of the stopping power incorporated in our σ_x values are listed in Tables I–IV.

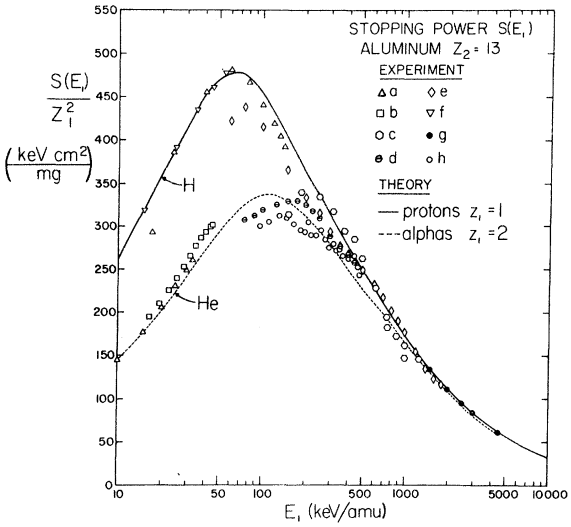

FIG. 2. Stopping-power curves for Al based on data a–h from Refs. 21–28, respectively. The curves marked "Theory" are obtained by the interpolation scheme, Eq. (6)ff. discussed in the text.

For the remaining quantity required in the calculation of cross sections, viz., the absorption

TABLE II. Aluminum K-shell x-ray production cross sections $\sigma_x(E_1)$ for incident deuterons of energies E_1. Column 2 is the measured thick-target x-ray yield $Y(E_1)$ and fitted yield $Y_f(E_1)$ in x rays per incident particle; $Y(E_1)$ is calibrated with our proton yields, Table I. Column 3 is the slope of the excitation function. Column 4 is the stopping power of aluminum for $^2_1$D. Column 5 is the x-ray production cross section, in barns, as determined by Eq. (5) with $n = 2.23 \times 10^{19}$ atoms/mg and $\mu = 391$ cm^2/g. Numbers in parentheses indicate powers of 10. K-shell ionization cross sections are $\sigma_K^{\text{expt}} = \gamma_K^{-1}\sigma_x$.

Energy E_1 (MeV) ± 0.5%	Al(K) x-ray yield $Y(E_1)$ x rays/particle ± 3%	$Y_f(E_1)$	$dY_f(E_1)/dE_1$ x rays/keV particle ± 15%	$S(E_1)$ (keV cm^2/mg) ± 10%	$\sigma_x(E_1)$ (b) ± 25%
4.00(−2)	6.41(−10)	6.28(−10)	1.04(−10)	357	1.68(−3)
4.50(−2)	1.33(− 9)	1.35(− 9)	1.92(−10)	375	3.25(−3)
5.00(−2)	2.53(− 9)	2.62(− 9)	3.24(−10)	390	5.71(−3)
6.00(−2)	7.81(− 9)	7.86(− 9)	7.68(−10)	415	1.44(−2)
7.00(−2)	2.07(− 8)	1.90(− 8)	1.52(− 9)	435	3.00(−2)
8.00(−2)	3.91(− 8)	3.95(− 8)	2.66(− 9)	452	5.46(−2)
9.00(−2)	7.12(− 8)	7.38(− 8)	4.28(− 9)	462	9.00(−2)
1.00(−1)	1.22(− 7)	1.27(− 7)	6.45(− 9)	472	1.39(−1)
1.10(−1)	2.07(− 7)	2.05(− 7)	9.28(− 9)	476	2.02(−1)
1.20(−1)	3.16(− 7)	3.15(− 7)	1.28(− 8)	478	2.80(−1)
1.30(−1)	4.60(− 7)	4.65(− 7)	1.73(− 8)	480	3.81(−1)
1.40(−1)	6.90(− 7)	6.63(− 7)	2.27(− 8)	478	4.98(−1)
1.60(−1)	1.24(− 6)	1.25(− 6)	3.70(− 8)	472	8.05(−1)
1.80(−1)	2.21(− 6)	2.18(− 6)	5.71(− 8)	463	1.22(0)
2.00(−1)	3.45(− 6)	3.59(− 6)	8.49(− 8)	453	1.79(0)
2.20(−1)	5.75(− 6)	5.64(− 6)	1.23(− 7)	442	2.54(0)
2.40(−1)	8.77(− 6)	8.58(− 6)	1.73(− 7)	432	3.50(0)
2.60(−1)	1.24(− 5)	1.27(− 5)	2.41(− 7)	423	4.79(0)
2.80(−1)	1.84(− 5)	1.84(− 5)	3.29(− 7)	413	6.42(0)

coefficient μ of the target for its own characteristic x rays, we have used the value $\mu = 391$ cm^2/g as measured by Bearden.[29] This value is in agreement with our measurements of the diminution factor of Al foils for Al (K) radiation.

The sources and the propagation of errors in determining the x-ray production cross section from the measurement of the thick-target x-ray yield can be summarized as follows. The error in the measured thick-target x-ray yield is ± 3%. This derives from a 2% error in the measurements of the incident ion dose and a 1% statistical uncertainty in the counting of the emitted x rays. With the methods of thick-target yield data analysis outlined above, we conclude that the slope of the excitation function can be determined to an accuracy of ± 15%. We assign an over-all uncertainty of ± 10% to the stopping power of aluminum and a similar uncertainty to the mass absorption coefficient of aluminum for its own characteristic x rays. In summary, we find that the x-ray production cross sections $\sigma_x(E_1)$, which range here over seven orders of magnitude, can be determined at each E_1 from thick-target yield measurements to an accuracy of ± 20–30%. We mention parenthetically that this error can be reduced by a factor of 10 with thin targets in transmission experiments, because stopping power and self-absorption do not enter into the data reduction. Transmission experiments at low velocities are not feasible because of low x-ray yields and the lack of target stability.

Tables I–IV present our Al (K) x-ray production cross sections for $^1_1$H, $^2_1$D, $^3_2$He, and $^4_2$He projectiles incident on aluminum. Figure 3 displays the cross sections for protons with energies ranging from 0.1 to 3 MeV. They agree within experimental errors with results obtained by other investigators where the data overlap in energy.[5,30,31]

TABLE III. Aluminum K-shell x-ray production cross sections $\sigma_x(E_1)$ for incident $^3_2$He particles of energies E_1. Column 2 is the measured thick-target x-ray yield $Y(E_1)$ and fitted yield $Y_f(E_1)$ in x rays per incident particle; calibration as in Table II. Column 3 is the slope of the excitation function. Column 4 is the stopping power of aluminum for incident $^3_2$He particles. Column 5 is the x-ray production cross section, in barns, as determined by Eq. (5) with $n = 2.23 \times 10^{19}$ atoms/mg and $\mu = 391$ cm^2/g. Numbers in parentheses indicate powers of 10. K-shell ionization cross sections are $\sigma_K^{\text{expt}} = \gamma_K^{-1}\sigma_x$.

Energy E_1 (MeV) ± 0.5%	Al(K) x-ray yield $Y(E_1)$ x rays/particle ± 3%	$Y_f(E_1)$	$dY_f(E_1)/dE_1$ x rays/keV particle ± 15%	$S(E_1)$ (keV cm^2/mg) ± 10%	$\sigma_x(E_1)$ (b) ± 25%
4.50(−2)	1.83(−11)	1.81(−11)	3.92(−12)	706	1.24(−4)
5.00(−2)	5.06(−11)	5.38(−11)	9.81(−12)	740	3.26(−4)
6.00(−2)	3.22(−10)	2.92(−10)	3.52(−11)	810	1.28(−3)
7.00(−2)	1.04(− 9)	1.03(− 9)	1.02(−10)	865	3.97(−3)
8.00(−2)	2.72(− 9)	2.75(− 9)	2.31(−10)	920	9.58(−3)
9.00(−2)	5.97(− 9)	6.08(− 9)	4.00(−10)	968	1.75(−2)
1.00(−1)	1.17(− 8)	1.18(− 8)	7.15(−10)	1020	3.29(−2)
1.10(−1)	1.96(− 8)	2.06(− 8)	1.07(− 9)	1060	5.12(−2)
1.20(−1)	3.22(− 8)	3.36(− 8)	1.53(− 9)	1092	7.55(−2)
1.40(−1)	7.83(− 8)	7.60(− 8)	2.78(− 9)	1150	1.45(−1)
1.60(−1)	1.55(− 7)	1.48(− 7)	4.47(− 9)	1200	2.43(−1)
1.80(−1)	2.56(− 7)	2.61(− 7)	6.89(− 9)	1240	3.88(−1)
2.00(−1)	4.60(− 7)	4.30(− 7)	1.00(− 8)	1312	5.96(−1)
4.08(−1)	1.14(− 5)	1.17(− 5)	1.35(− 7)	1334	8.28(0)
5.10(−1)	3.36(− 5)	3.38(− 5)	3.18(− 7)	1328	1.95(1)
6.12(−1)	7.58(− 5)	8.13(− 5)	6.40(− 7)	1240	3.70(1)
7.14(−1)	1.75(− 4)	1.71(− 4)	1.15(− 6)	1200	6.49(1)
8.16(−1)	3.25(− 4)	3.23(− 4)	1.88(− 6)	1132	1.01(2)
1.02(0)	9.21(− 4)	9.13(− 4)	4.09(− 6)	1062	2.11(2)
1.12	1.48(− 3)	1.40(− 3)	5.57(− 6)	1022	2.80(2)
1.22	2.10(− 3)	2.06(− 3)	7.33(− 6)	992	3.62(2)
1.43	3.82(− 3)	3.96(− 3)	1.15(− 5)	940	5.54(2)
1.63	6.67(− 3)	6.79(− 3)	1.63(− 5)	884	7.65(2)
1.84	1.14(− 2)	1.07(− 2)	2.18(− 5)	844	1.01(3)
2.04	1.58(− 2)	1.58(− 2)	2.76(− 5)	802	1.27(3)
2.24	2.23(− 2)	2.21(− 2)	3.44(− 5)	770	1.57(3)
2.45	2.95(− 2)	2.99(− 2)	4.16(− 5)	736	1.90(3)
2.65	3.88(− 2)	3.91(− 2)	4.88(− 5)	706	2.22(3)
2.85	5.03(− 2)	4.99(− 2)	5.60(− 5)	680	2.58(3)
2.96	5.72(− 2)	5.57(− 2)	5.95(− 5)	670	2.76(3)

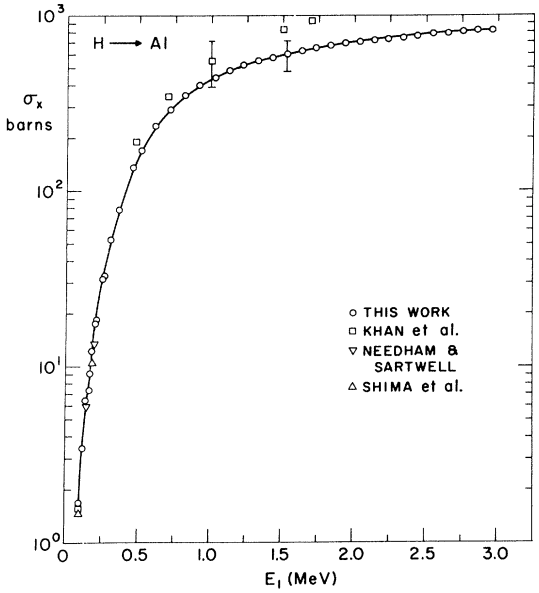

FIG. 3. Thick-target cross sections for Al(K) x-ray production by protons as a function of incident energy E_1. The curve is experimental, cf. Table I. Other data are those of Khan *et al.* (Ref. 5), Needham and Sartwell (Ref. 30), and Shima *et al.* (Ref. 31).

III. THEORY IN PLANE-WAVE BORN APPROXIMATION

A. Born Series

The nonrelativistic ionizing collision between a charged particle and an atom can be described by a Hamiltonian of the form

$$H = H_0 + gU_0 + hV_0 , \tag{11}$$

where H_0 denotes the noninteracting particle-atom system, gU_0 is the Coulomb interaction of strength g between the particle and the atomic nucleus, and hV_0 is the ionizing Coulomb interaction of strength h between the particle and the atomic electrons. Both h and g are proportional to the particle charge Q_1. The ionization cross section for this process can be expanded, in principle,[32] into a Born series in powers of h:

$$\sigma = \sum_{\nu=2}^{\infty} h^\nu G_\nu(g). \tag{12}$$

The terms $h^\nu G_\nu(g)$ are related to the matrix elements of hV_0 between the eigenstates of $H_0 + gU_0$. The leading term, of order h^2,

$$\sigma^{\mathrm{CWBA}} \equiv h^2 G_2(g) , \tag{13}$$

is the Born approximation to the Born series Eq. (12) for the exact cross section. It may be termed the (first) "Coulomb-wave Born approximation" (CWBA) because $G_2(g)$ depends on the eigenstates of $H_0 + gU_0$ which are products of unperturbed target atomic states and states describing the particle as a scattered Coulomb wave. Equation (12) is then the Coulomb-wave Born series.

Each coefficient $G_\nu(g)$ in Eq. (12) can be expanded in a power series in g with coefficients $J_{\mu\nu}$ which are related to matrix elements of U_0 and V_0 between the eigenstates of H_0. These eigenstates are products of unperturbed target atomic states and unperturbed particle plane-wave states. The expansion takes the form

$$\sigma = \sum_{\nu=2}^{\infty} \sum_{\mu=0}^{\infty} g^\mu h^\nu J_{\mu\nu} . \tag{14}$$

The double sum in Eq. (14) is thus a plane-wave Born series in powers of the strengths of the total interaction $gU_0 + hV_0$ between particle and atom. Retaining the first term yields the (first) "plane-wave Born approximation" (PWBA)

$$\sigma^{\mathrm{PWBA}} \equiv h^2 J_{02} = h^2 \, G_2(g = 0) \tag{15}$$

to the exact σ, because J_{02} depends only on the eigenstates of H_0 which describe the incoming particle as a plane wave. The atomic states are the same for either series [Eq. (12) or (14)].

For a particle of specific charge $Z_1 e$, Eq. (15) implies that σ and σ^{PWBA} are interrelated as

$$\sigma^{\mathrm{PWBA}} = Z_1^2 \, \Gamma, \tag{16}$$

where

$$\Gamma = \lim_{Q_1 \to 0} [\sigma(Q_1)/Q_1^2]. \tag{17}$$

For all target atoms at all particle velocities, the PWBA to the ionization cross section σ is equal to Z_1^2 times Γ, the exact ionization cross section per particle charge squared *in the limit of vanishingly small particle charge* Q_1. The quantum theory of inner-shell ionization has been developed extensively in this approximation.

Valid application of the theory with the Hamiltonian Eq. (11) requires that:

(i) The projectile acts as a point charge.

This will be the case for projectiles whose electronic structure makes a negligible effect on the ionization process.

Application of the PWBA in place of the complete theory for Eq. (11) rests on the basic assumption that the term given by Eq. (15) dominates all other terms in the series expansion in Eq. (14). This is guaranteed in the limit of vanishingly small particle charge as defined by Eqs. (16) and (17). This limit requires that:

(ii) The initial and final particle waves are planar over all space;

(iii) the states of the target electrons are those of the unperturbed target.

When requirements (i)–(iii) are fulfilled, the ability to calculate realistic σ values to compare

with experiment is limited solely by the quality of available approximations to the exact eigenfunctions of H_0.

Requirement (i) is valid for $Z_1 \ll Z_2$ at low velocities $v_1 \ll \frac{1}{2}\theta_K v_{2K}$ for reasons described in Sec. I. In most targets this requirement is met also at higher velocities because stripping of the projectile K shell occurs when $v_1 \gg Z_1 v_0$ which is $v_1 \gg (Z_1/Z_{2K})v_{2K}$. Thus, as long as

$$Z_1/Z_2 \ll 1, \tag{18}$$

projectiles act as bare point charges at any velocity and, as regards requirement (i), the theory of Coulomb excitation developed from Eq. (11) applies.

Use of the PWBA, as defined by Eqs. (16) and (17), is qualified by the fact that in the laboratory ionization cross sections are measured with projectiles of finite charge $Q_1 = Z_1 e$, and thus terms higher in order than Eq. (15) may contribute. It is usually assumed that the limit $Q_1 \to 0$ can be imitated sufficiently well by restricting the range of target elements such that $Z_1 e/Q_2 \ll 1$, where Q_2 is the charge governing the atomic eigenstates of H_0 between which the target transitions take place. For K-shell ionization

TABLE IV. Aluminum K-shell x-ray production cross sections $\sigma_x(E_1)$ for incident $^4_2$He particles of energies E_1. Column 2 is the measured thick-target x-ray yield $Y(E_1)$ and fitted yield $Y_f(E_1)$ in x rays per incident particle; calibration as in Table II. Column 3 is the slope of the excitation function. Column 4 is the stopping power of aluminum for $^4_2$He particles. Column 5 is the x-ray production cross section, in barns, as determined by Eq. (5) with $n = 2.23 \times 10^{19}$ atoms/mg and $\mu = 391$ cm^2/g. Numbers in parentheses indicate powers of 10. K-shell ionization cross sections are $\sigma_K^{\text{expt}} = \gamma_K^{-1}\sigma_x$.

Energy E_1 (MeV) ± 0.5%	Al(K) x-ray yield $Y(E_1)$ x rays/particle ± 3%	$Y_f(E_1)$	$dY_f(E_1)/dE_1$ x rays/keV particle ± 15%	$S(E_1)$ (keV cm^2/mg) ± 10%	$\sigma_x(E_1)$ (b) ± 25%
6.00(−2)	3.34(−11)	3.32(−11)	6.60(−12)	706	2.10(−4)
7.00(−2)	1.29(−10)	1.31(−10)	2.15(−11)	760	7.35(−4)
8.00(−2)	4.26(−10)	4.29(−10)	4.80(−11)	810	1.75(−3)
9.00(−2)	1.19(− 9)	1.16(− 9)	1.06(−10)	850	4.06(−3)
1.00(−1)	2.76(− 9)	2.69(− 9)	1.90(−10)	892	7.65(−3)
1.20(−1)	9.42(− 9)	1.00(− 8)	4.80(−10)	968	2.10(−2)
1.40(−1)	2.69(− 8)	2.65(− 8)	1.02(− 9)	1032	4.77(−2)
1.60(−1)	5.75(− 8)	5.67(− 8)	1.70(− 9)	1092	8.42(−2)
1.80(−1)	1.08(− 7)	1.10(− 7)	2.91(− 9)	1140	1.50(−1)
2.00(−1)	1.87(− 7)	1.92(− 7)	4.50(− 9)	1175	2.41(−1)
4.08(−1)	5.39(− 6)	5.09(− 6)	5.22(− 8)	1352	3.25(0)
5.10(−1)	1.21(− 5)	1.29(− 5)	1.06(− 7)	1340	6.60(0)
6.12(−1)	2.79(− 5)	2.82(− 5)	2.04(− 7)	1312	1.25(1)
7.14(−1)	6.01(− 5)	5.75(− 5)	3.83(− 7)	1280	2.30(1)
8.16(−1)	1.11(− 4)	1.09(− 4)	6.45(− 7)	1240	3.78(1)
1.02(0)	3.18(− 4)	3.20(− 4)	1.50(− 6)	1176	8.47(1)
1.12	4.89(− 4)	5.04(− 4)	2.12(− 6)	1140	1.17(2)
1.22	7.53(− 4)	7.56(− 4)	2.85(− 6)	1104	1.54(2)
1.43	1.48(− 3)	1.52(− 3)	4.71(− 6)	1048	2.48(2)
1.63	2.75(− 3)	2.71(− 3)	7.04(− 6)	996	3.62(2)
1.84	4.58(− 3)	4.42(− 3)	9.81(− 6)	948	4.95(2)
2.04	6.90(− 3)	6.74(− 3)	1.30(− 5)	906	6.46(2)
2.24	9.28(− 3)	9.75(− 3)	1.66(− 5)	872	8.20(2)
2.35	1.19(− 2)	1.15(− 2)	1.85(− 5)	860	9.15(2)
2.45	1.29(− 2)	1.35(− 2)	2.06(− 5)	844	1.02(3)
2.55	1.68(− 2)	1.58(− 2)	2.30(− 5)	832	1.14(3)
2.65	1.78(− 2)	1.82(− 2)	2.53(− 5)	816	1.25(3)
2.85	2.59(− 2)	2.48(− 2)	2.99(− 5)	784	1.49(3)
2.96	2.85(− 2)	2.79(− 2)	3.15(− 5)	776	1.59(3)
3.06	3.16(− 2)	3.12(− 2)	3.31(− 5)	760	1.68(3)
3.16	3.45(− 2)	3.47(− 2)	3.45(− 5)	744	1.76(3)
3.26	3.81(− 2)	3.82(− 2)	3.57(− 5)	736	1.85(3)
3.67	5.18(− 2)	5.36(− 2)	3.94(− 5)	700	2.18(3)
4.08	6.76(− 2)	7.01(− 2)	4.10(− 5)	656	2.44(3)
4.69	9.29(− 2)	9.51(− 2)	4.00(− 5)	608	2.76(3)
5.51	1.24(− 1)	1.26(− 1)	3.42(− 5)	580	3.10(3)
5.92	1.44(− 1)	1.39(− 1)	3.01(− 5)	540	3.17(3)

$Q_2 = Z_{2K}e$. Thus $Q_1 \to 0$ is taken to be simulated by $Z_1/Z_2 \ll 1$ which is sufficient to satisfy requirement (i). Yet the restriction $Z_1/Z_2 \ll 1$ alone does not in general satisfy requirements (ii) and (iii).

Even if $Z_1/Z_2 \ll 1$, and hence $h \ll 1$, large deviations of σ^{PWBA} from σ can occur because rapid convergence of the Born series hinges on the coefficients $J_{\mu\nu}$ in Eq. (14). Valid application of the PWBA requires, in addition to $Z_1/Z_2 \ll 1$, that a number of other criteria are fulfilled with regard to particle velocity, particle mass, and target atomic number. It is well known that general criteria of this kind are difficult to formulate explicitly.[33] A criterion commonly invoked[4] for the validity of the PWBA is $v_1 \gg Z_1 v_0$ or, in terms of v_{2K},

$$v_1 \gg (Z_1/Z_{2K})v_{2K}. \tag{19}$$

This, in fact, constitutes the condition that the amplitude of the wave scattered by the target electron is negligible in comparison to that of the incident wave.[34] It pertains to requirement (ii) but cannot be the complete criterion because Coulomb scattering by the target nucleus is omitted. Equation (19) bears on requirement (i) since, by coincidence, it also gives the condition for the stripping of all electrons from the moving projectile.

One may take requirement (ii) to be satisfied when the Coulomb interaction between point charges Z_1e and Z_2e of reduced mass $M = (M_1^{-1} + M_2^{-1})^{-1}$, if repulsive, is so weak that one-half of the distance of closest approach in a head-on collision d,

$$d = \tfrac{1}{2}(Z_1 Z_2 e^2/\tfrac{1}{2}Mv_1^2) \simeq Z_1(m_e/M)(v_{2K}/v_1)^2 a_{2K}, \tag{20}$$

is small compared to q_0^{-1}, the optimum penetration distance for K-shell ionization.[1] That is,

$$v_1^3 \gg \tfrac{1}{2}\theta_K Z_1(m_e/M)v_{2K}^3 \tag{21}$$

ensures a negligible effect of Coulomb deflection.

The K-shell orbits will not be distorted by the passing particle if the electron response time ω_{2K}^{-1} is long compared to the particle-electron interaction time $\simeq a_{2K}/v_1$; i.e., requirement (iii) is fulfilled for

$$v_1 \gg \omega_{2K} a_{2K} = \tfrac{1}{2}\theta_K v_{2K} \tag{22}$$

which, by Eq. (1), covers the high-velocity domain.

As long as $Z_1 \lesssim Z_2$, a hierarchy of conditions obtains: Eq. (22) → Eq. (19) → Eq. (21). If the connection between the stripping condition [Eq. (19)] and requirement (i) is used, this logical chain may be expressed in terms of requirements (i)–(iii) as: (iii) → (i) → (ii).

In summary, the PWBA as employed for the calculation of cross sections for K-shell ionization by heavy charged particles is a theory for particles of small charges and high velocities which can break down by a hierarchy of conditions for real projectiles at low velocities. In fact, we find that, if $(\tfrac{1}{2}\theta_K) \lesssim v_1/v_{2K} \lesssim 1$, polarization effects of the atomic states can contribute, as will be discussed in Paper II; if $v_1/v_{2K} \lesssim (\tfrac{1}{2}\theta_K)$, the penetrating particle changes the binding energies of the target electrons[6,7]; moreover, if $v_1^3/v_{2K}^3 \lesssim \tfrac{1}{2}\theta_K Z_1(m_e/M)$, Coulomb deflection of the particle in the field of the target nucleus prevents deep K-shell penetration.[6,7] The experimental data reveal significant deviations from the PWBA predictions in these velocity domains. They can be traced quantitatively to effects caused by the finite particle charge. These effects are not contained in the PWBA.

B. Choice of Wave Functions

Before the predictions of the PWBA can be subjected to meaningful experimental scrutiny, we must demonstrate that the calculated σ_K^{PWBA} are not in serious error simply because we have only approximate wave functions to evaluate them. To this end, we studied the sensitivity of σ_K^{PWBA} to the choice of "best" wave functions by computing cross sections for two sets of approximate K-shell eigenfunctions.[35] One comprises the screened hydrogenic wave functions (H) ordinarily employed in such calculations.[36] The other derives from self-consistent central atomic potentials determined numerically from a Hartree–Slater (HS) approach.[37] For the HS set, partial-wave contributions σ_l corresponding to the angular momentum quantum number l of the final electron continuum state, must be computed term by term to obtain

$$\sigma_K^{\mathrm{PWBA}}(\mathrm{HS}) = \sum_{l=0}^{\infty} \sigma_{K,l}^{\mathrm{PWBA}}(\mathrm{HS}). \tag{23}$$

Detailed calculations of the K-shell ionization cross sections with H wave functions evince the dominance of the s-wave term, $l = 0$, over all other terms in the sum at particle velocities $v_1 \ll v_{2K}$.[38] The p-wave term, $l = 1$, dominates when $v_1 \gg v_{2K}$. At intermediate velocities $v_1 \simeq v_{2K}$, the s and p terms contribute some 70% to the total cross section. The terms $l > 1$ are neglected in this subsection.

The cross sections computed for Al ($Z_2 = 13$) and Cu ($Z_2 = 29$) from H and HS wave functions do not differ significantly (cf. Fig. 4 for Al). This result is linked to the circumstance, of course, that the electron environment in the K shell is dominated by the nuclear Coulomb field and, therefore, the HS wave functions are essentially hydrogenic in character. Thus the HS atomic potential differs significantly from a pure Coulomb potential at distances larger than a_{2K}. But there both H and HS wave functions are small and contribute little to the radial integrations. By contrast, H and HS cross sections for L-shell ionizations can, under certain circumstances, differ appreciably.[39]

We infer from this study that PWBA K-shell cross sections calculated with hydrogenic wave

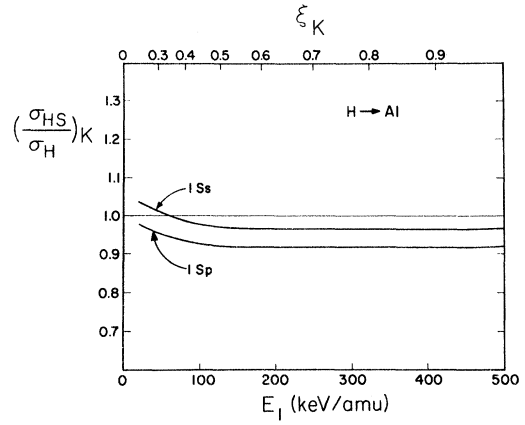

FIG. 4. Calculated ratios of the Hartree–Slater (HS) cross sections to hydrogenic (H) cross sections for Al(K) ionization transitions to the s-wave continuum ($1Ss$) and to the p-wave continuum ($1Sp$). The deviations from the straight line at unity are an indication of the residual dependence on the choice of wave functions.

functions can differ only negligibly from the exact σ_K^{PWBA}. The causes for discrepancies between theory and experiment must be sought in the breakdown of the PWBA under the conditions of the experiment.

C. Predictions

The nonrelativistic PWBA predicts a particular universal form for the ionization cross sections. With $h \equiv Z_1/Z_2$ for K-shell ionization [cf. Eq. (11)] one can rewrite Eq. (15) as

$$\sigma_K^{\mathrm{PWBA}} = Z_1^2 (G_2(0)/Z_2^2) \equiv Z_1^2 F_2(\xi_K) \tag{24}$$

to obtain a function $F_2(\xi_K)$ that depends on target and particle via the minimum momentum transfer $\hbar q_0$ which appears through the lower limit in the integration over all momentum transfers for a given energy transfer.[4]

Equation (24) states that the cross section divided by Z_1^2 is the same for all particles incident with identical velocity on a given target atom. This prediction can be tested without knowledge of the function F simply by plotting cross-section data $\sigma_K^{\mathrm{expt}}/Z_1^2$ for a variety of particles against v_1, η_K, Eq. (2), or the universal variable ξ_K, Eq. (1). Such data should fall along a single curve. The comparison of the locus of this curve with calculations of the function $F_2(\xi_K)$, moreover, provides a test of the quantitative aspects of the theory.

The dependence of the cross sections on the target, apart from the scaling through $\xi_K = v_1/a_{2K}\omega_{2K}$, appears in F_2 as a parametric dependence on $\theta_K = 2\omega_{2K}/Z_{2K}^2$ (a.u.). To bring out target features, it is convenient to introduce the cross section

$$\sigma_{0K} \equiv 8\pi a_{2K}^2 (Z_1/Z_{2K})^2 \tag{25}$$

as a suitable unit for the scaling of K-shell cross sections. It can be viewed as a wave-mechanical cross section $4\pi a_{2K}^2$ for each of the two electrons in the shell, weighted by the square of the relative Coulomb-interaction strength. With Eqs. (2) and (25), Eq. (24) can be recast as

$$\sigma_K^{\mathrm{PWBA}}(\eta_K; \theta_K) = Z_1^2 F_2(\xi_K) \equiv \sigma_{0K} f(\eta_K/\theta_K^2; \theta_K)/\eta_K. \tag{26}$$

θ_K appears in the function f in combination with η_K as a universal variable $\eta_K/\theta_K^2 = (\frac{1}{2}\xi_K)^2$ and as an independent parameter. Even though the variation of θ_K with Z_2 represents an implicit parametric dependence of the reduced cross section $\sigma_K^{\mathrm{PWBA}}/\sigma_{0K}$ on the target, by virtue of the transformation[4]

$$(a\,y)^{-1} f(y; a) = y^{-1} f(y; 1) \equiv F(y), \tag{27}$$

one can still scale the cross sections, because the right-hand side of Eq. (27) is a function of $y = \eta_K/\theta_K^2$ only. The universal function $F(y)$ is tabulated in Table V and displayed in Figs. 5 and 7. Equation (27) is exact when $y \ll 1$, is a good approximation near $y \simeq 1$, but begins to become less accurate than the experiments when $y \gg 1$. The PWBA prediction of K-shell ionization cross sections can be stated concisely: The reduced ionization cross section

$$\sigma_K^{\mathrm{PWBA}}(\eta_K; \theta_K)/(\sigma_{0K}/\theta_K) = F(\eta_K/\theta_K^2) \tag{28}$$

depends only on the variable η_K/θ_K^2. The inconsequential limitation of Eq. (27) aside, the role of θ_K is merely that of a scale factor.

TABLE V. The universal function $F(y)$ for calculating K-shell cross sections as a function of the particle-velocity variable η_K, Eq. (2). In the PWBA, one sets $y = \eta_K/\theta_K^2$, cf. Eq. (28). The cross section including the binding effect is obtained by setting $y = \eta_K/(\epsilon\theta_K)^2$, cf. Eq. (40), where $\epsilon\theta_K$ is given by Eq. (37) in conjunction with Table VI or Eq. (39). $F(y)$ is shown in Figs. 5 and 7. Although based on values for aluminum (Ref. 36), this table predicts, by Eq. (27), the nonrelativistic K-shell ionization cross sections for all particle-target pairs with $Z_1 \ll Z_2$ at particle velocities such that $y < 10$.

y	$F(y)$	y	$F(y)$
6.796(−3)	5.183(−6)	6.686(−1)	5.773(−1)
9.581(−3)	1.904(−5)	8.464(−1)	6.530(−1)
1.381(−2)	7.386(−5)	1.026(0)	6.999(−1)
2.099(−2)	3.299(−4)	1.207(0)	7.271(−1)
2.828(−2)	9.158(−4)	1.389(0)	7.409(−1)
4.317(−2)	3.573(−3)	1.755(0)	7.435(−1)
5.836(−2)	8.751(−3)	2.124(0)	7.278(−1)
7.381(−2)	1.671(−2)	2.494(0)	7.043(−1)
8.946(−2)	2.737(−2)	2.681(0)	6.915(−1)
1.213(−1)	5.569(−2)	3.054(0)	6.641(−1)
1.536(−1)	9.093(−2)	3.616(0)	6.250(−1)
2.362(−1)	1.924(−1)	5.503(0)	5.108(−1)
3.206(−1)	2.939(−1)	9.315(0)	3.736(−1)
4.930(−1)	4.614(−1)	1.315(1)	2.946(−1)

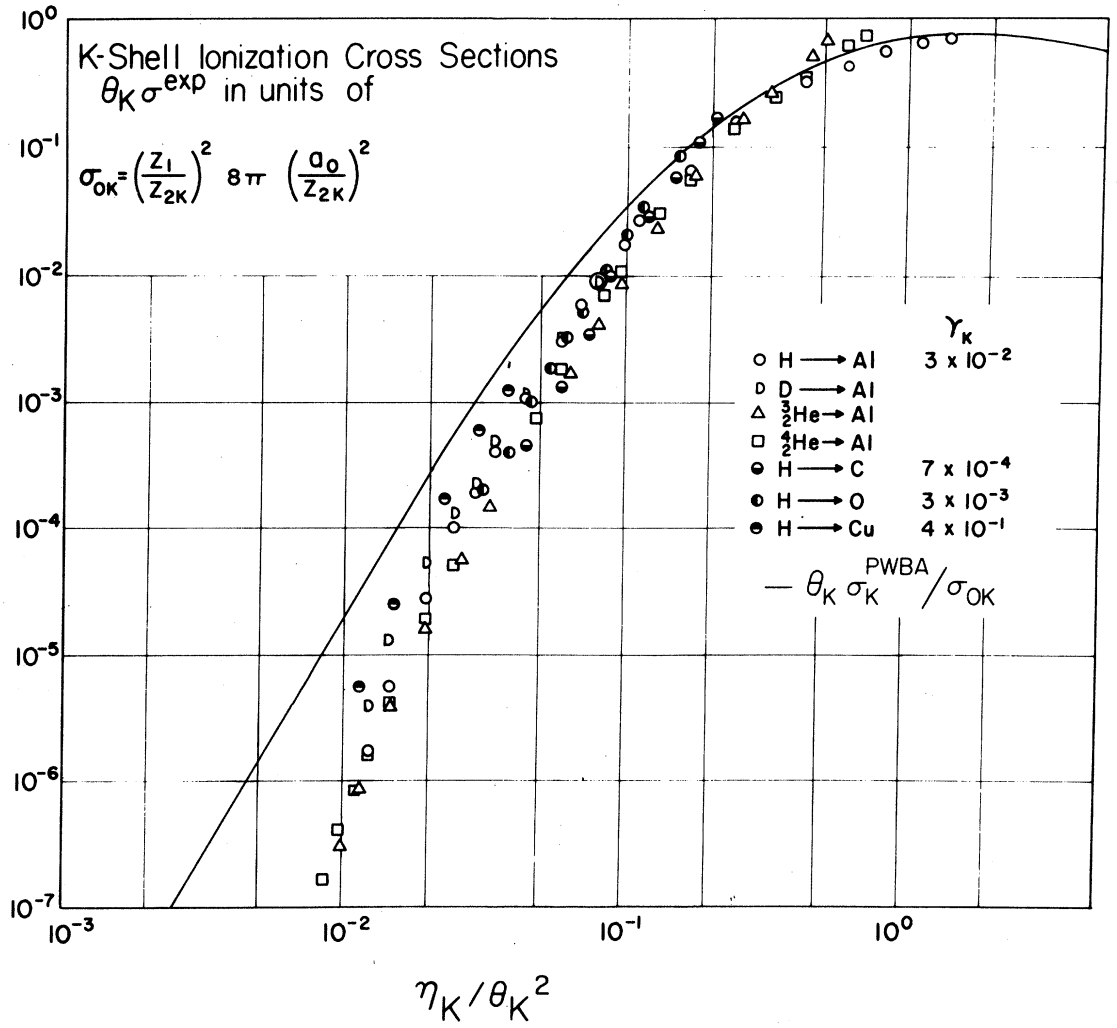

FIG. 5. K-shell ionization cross sections in a scaled plot as prescribed by the PWBA, Eq. (28). The data do not form a universal curve, and the calculated curve disagrees with the data. The data for Al stem from the present work and Refs. 7 and 8. The other data are taken from Refs. 5 and 9.

All cross sections should follow a universal curve if reduced as prescribed on the left-hand side of Eq. (28) and plotted versus ξ_K or η_K/θ_K^2. This assertion of universality can be tested on data measured with different particles impinging at various energies on different targets without any explicit knowledge of the function F. Examination of the locus of such reduced data and comparison with calculated values of F can assess the validity ranges of the assumptions leading from first principles to the predictions of universality and of the absolute magnitude of the cross sections.

IV. COMPARISON WITH EXPERIMENT

The technique of determining characteristic K-shell x-ray yields under projectile bombardment provides a measure of the cross section for x-ray production σ_x, as described in Sec. II. The theory, on the other hand, predicts ionization cross sections σ_K. The two cross sections are related by the fluorescence yield γ_K. It accounts for the fraction of K-shell holes created in the ionization process that subsequently are filled with electrons under the emission of characteristic K x rays. The remaining fraction of holes $1-\gamma_K$ is filled by Auger processes. Since the contribution of the narrow range of excited bound states to the sum over final states is negligible compared to that of ionized states, the relation

$$\sigma_K^{expt} = \gamma_K^{-1} \sigma_x \tag{29}$$

is taken to determine the experimental K-shell ionization cross section σ_K^{expt}. Since the fluorescence time normally is long compared to collision times, the fluorescence yield is uninfluenced by the presence of the projectile. Corresponding values of γ_K

are available from experiment and theory.[40]

Experimental cross sections σ_K^{expt} for a variety of projectiles and targets are plotted in reduced form in Fig. 5 as prescribed by Eq. (28). Two significant discrepancies are apparent:

(i) The reduced cross sections at the same value of η_K/θ_K^2 scatter widely. The spread grows with decreasing η_K/θ_K^2 to nearly one order of magnitude on the ordinate scale.

(ii) The experimental cross sections consistently fall below the calculated PWBA values. The gap between theory and experiment grows with decreasing η_K/θ_K^2 and can exceed one order of magnitude.

We conclude:

(a) PWBA cross sections account only crudely for the trends with particle velocity.

(b) The PWBA predictions of universality and of the magnitudes are in error.

In view of long-standing difficulties in determining convergence conditions for Born series involving inelastic processes, it is important to note that an empirical condition for the convergence of Eq.

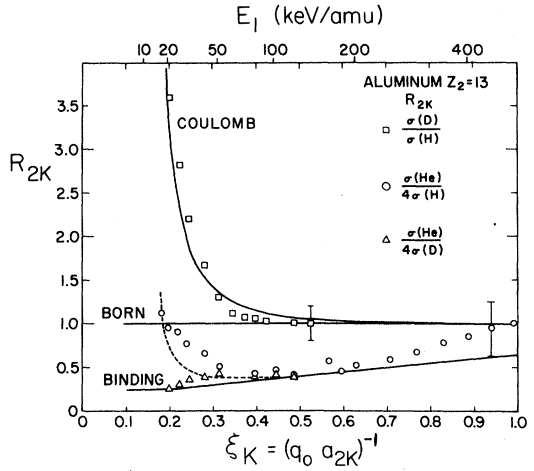

FIG. 6. Al(K) ionization cross-section ratios, Eq. (30), for various projectile pairs. The theoretical curves show ratios of cross sections given by Eq. (42) and formed as stipulated in Eq. (30). The straight line at unity marked BORN is the prediction in PWBA. As in the case of isotope pair $^4_2$He, $^3_2$He published earlier (Ref. 8), the upper solid curve marked COULOMB applies to the isotope pair $^2_1$D, $^1_1$H. It depicts the ratio of the respective Coulomb deflection factors $[9E_{10}(^2_1\mathrm{D})/9E_{10}(^1_1\mathrm{H})]_{\mathrm{Al}}$, because the corresponding cross sections σ_K^B, Eq. (40), cancel for isotopes. The lower solid curve marked BINDING shows the reduction, relative to R_{2K}^{PWBA}, of R_{2K} as predicted for the pair $^4_2$He, $^2_1$D of equal charge-to-mass ratio. In effect it is a graph of $[\sigma_K^B(^4_2\mathrm{He})/4\sigma_K^B(^2_1\mathrm{D})]_{\mathrm{Al}}$ since the Coulomb-deflection factors essentially cancel for such pairs. The dashed curve depicts the ratio of the cross sections for the pair $^4_2$He, $^1_1$H as calculated from Eq. (42). It exhibits the competing influences of the Coulomb deflection and binding effects at very low particle velocities.

(14) to the PWBA term, Eq. (15), may be obtained by inspection of Fig. 5. For instance, at $\eta_K/\theta_K^2 = 0.05$, the PWBA cross section is roughly twice as large as the experimental cross section. Since $0.6 < \theta_K < 1$, this corresponds to $v_1 \simeq 0.2\ v_{2K}$ and an "observed" criterion for the convergence of the Born series for K-shell ionization could be taken to be $v_1 \gg 0.2\ v_{2K}$. When this condition is not met the PWBA cross section can fail by factors of 2 or more. For $Z_1 \ll Z_2$, as is the case for the data, this criterion is consistent with the condition of Eq. (19).

The lack of universality of the data can be brought into sharper focus by plotting ratios R_{2K} of cross sections of a given target for pairs of particles Z_1 and Z_1' versus the particle velocity as shown in Fig. 6. For definiteness, the ratios are formed such that $Z_1 < Z_1' \ll Z_2$ or, if isotopes $Z_1 = Z_1'$, such that $M_1 < M_1' \ll M_2$. The ratios are formed according to

$$R_{2K} \equiv [\sigma_K(Z_1')/Z_1'^2][\sigma_K(Z_1)/Z_1^2]^{-1}. \tag{30}$$

It follows from Eq. (26) that $R_{2K}^{PWBA} = 1$. Ratios offer a sensitive way of comparing dependences on projectile properties because they largely cancel uncertainties in the calibrations and the fluorescence yields, and because they permit inspection of deviations on a linear scale over the six–seven orders of magnitude in experimental cross sections now available. The measured R_{2K} do not agree with the PWBA value.[6–8,12,13,31]

Even before turning to their quantitative analysis, in Sec. V, the discrepancies can be understood qualitatively in terms of important physical effects not appearing in the PWBA. One effect is the Coulomb deflection of the particle in the field of the target nucleus, which is neglected in the step from Eq. (13) to (15). The deflection obstructs deep particle penetration into the K shell and reduces the likelihood of ionization, the more so the lower the particle velocity. Of two isotopes (e.g., $^2_1$D, $^1_1$H, or $^4_2$He, $^3_2$He) with the same velocity, the heavier particle penetrates deeper into the K shell. Therefore, R_{2K} shows a pronounced isotope effect in the form of a rapid rise with decreasing particle velocity. As a corollary, pairs of different particles with the same charge-to-mass ratio (e.g., $^4_2$He, $^2_1$D or $^6_3$Li, $^2_1$D) undergo equal Coulomb deflections in the field of a heavy target nucleus. Therefore, their R_{2K} should not, and in fact do not, show a Coulomb upturn even at very low particle velocities (Fig. 6).

The effects of Coulomb deflection on the cross section become unimportant at still fairly low particle velocities, so that, for $\xi_K > 0.5$, they do not interfere with the analysis of the causes for deviations from the PWBA. These deviations derive from the dynamics of the target electrons under the influence of a passing charged particle. For isotopes such electronic effects virtually cancel in forming

R_{2K} at any velocity. For all pairs that are not isotopes, and after the Coulomb upturn has subsided for particle pairs of unequal charge-to-mass ratios, Fig. 6 reveals that R_{2K} is significantly smaller than $R_{2K}^{\mathrm{PWBA}}=1$, and that it approaches the line $R_{2K}^{\mathrm{PWBA}}=1$ slowly from below.

We attribute this effect to the influence of the incident particle on the atomic state from which ionization occurs.[6-8] Particles of low velocity such that $\xi_K \ll 1$ cause significant ionization only if they penetrate into the K shell with impact parameters of order $q_0^{-1}=v_1/\omega_{2K} \ll a_{2K}$. In so doing they remain inside the K shell for times a_{2K}/v_1 long compared to the K-shell time ω_{2K}^{-1}. The K-shell electrons can respond to the presence of the projectile near the nucleus. In effect, then, the electronic state from which ionization occurs is characterized not by the binding energy $\theta_K Z_{2K}^2 \mathcal{R}$ but, in the zero-velocity limit, by $\theta_K(Z_{2K}+Z_1)^2\mathcal{R}$. The latter reflects an increase of the binding of the electrons to the domain of the target K shell owing to the presence of the ionizing particle. To first order in Z_1/Z_{2K}, this increase in binding can be represented by a binding factor times $\theta_K Z_{2K}^2 \mathcal{R}$. In the low-velocity limit, this factor is seen to be the constant $1+2Z_1/Z_{2K}$. The factor approaches the value 1 as v_1 exceeds v_{2K}. The binding effect decreases the cross sections and their ratios in the way shown by the examples in Fig. 6. The curves represent theoretical predictions of the effects of particle Coulomb deflection and electronic binding as derived in the following Sec. V.

V. IMPROVEMENTS TO PWBA

A. Nuclear Coulomb Deflection

In their semiclassical treatment, Bang and Hansteen[1] calculate the K-shell ionization cross section by first-order time-dependent scattering theory under the assumption that the particle moves in the field of the target nucleus on a classical Coulomb-deflected hyperbolic trajectory. In the particle velocity range $\xi_K \ll 1$, the differential cross section for transfer of energy W (in units of $\frac{1}{2}Z_{2K}^2$ a.u.) can be written

$$\frac{d\sigma_K}{dW}=\frac{d\sigma_K^{\mathrm{PWBA}}}{dW}\, e^{-\pi dq_0 W/\theta_K}(1-\Delta), \tag{31}$$

where to lowest order in η_K,[41]

$$\frac{d\sigma_K^{\mathrm{PWBA}}}{dW}=\sigma_{0K}\frac{2^{17}}{5}\frac{\eta_K^4}{W^{10}} \quad \text{for} \quad \frac{\eta_K}{W^2}\ll 1\ . \tag{32}$$

The small correction Δ is omitted in the integration from $W=\theta_K$ to $W=\infty$, with the result[6,7]

$$\sigma_K = 9\,E_{10}(\pi dq_0)\sigma_K^{\mathrm{PWBA}}, \tag{33}$$

where $0\le 9E_{10}(x)\le 1$ for all $x\ge 0$. The function $E_{10}(x)=\int_1^\infty t^{-10}e^{-xt}dt$ is the exponential integral of order 10.[42] One can express the argument of E_{10} in terms of η_K/θ_K^2 as

$$\pi dq_0=(\tfrac{1}{2}\pi)\,Z_1(m_e/M)\theta_K^{-2}(\eta_K/\theta_K^2)^{-3/2}. \tag{33a}$$

The precise functional form of the Coulomb deflection factor $9E_{10}(\pi dq_0)$ applies at particle velocities so low that σ_K^{PWBA} approaches the asymptotic form corresponding to Eq. (32),

$$\frac{\sigma_K^{\mathrm{PWBA}}}{\sigma_{0K}/\theta_K}=\frac{2^{17}}{45}\left(\frac{\eta_K}{\theta_K^2}\right)^4 \quad \text{for} \quad \frac{\eta_K}{\theta_K^2}\ll 1\ , \tag{34}$$

which obeys the transformation Eq. (27) explicitly.

As an expedient, Eq. (33) with σ_K^{PWBA} as given by Eq. (26) is used to incorporate Coulomb deflection effects.[7] This procedure yields the proper limiting expressions: at velocities so high that Coulomb deflection effects vanish and $9E_{10}(\pi dq_0)\simeq 1$, one retrieves σ_K^{PWBA} [Eq. (26)]; at low velocities the cross section reduces to Eq. (33), with the asymptotic form of σ_K^{PWBA} [Eq. (34)] as derived from Eqs. (31) and (32).

The Coulomb deflection introduces, through Eq. (33a), a dependence of the cross section on the projectile mass, i.e., an isotope effect, as well as additional dependences on Z_1, θ_K, and η_K/θ_K^2. The influence of Coulomb deflection vanishes at projectile velocities such that $\pi dq_0 \ll 1$ as anticipated by Eq. (21).

B. Binding

The target K-shell electrons become more tightly bound to the K-shell region during the encounter with the particle because at low velocities it must penetrate to distances $\approx q_0^{-1} \ll a_{2K}$ deep within the K shell to cause ionization. As mentioned previously, under this condition the electron response time is much shorter than the collision time. This allows the electron to adjust to the presence of the projectile. The increased binding reduces the probability of ionization.[6,7] Our approach is related to a systematic development of time-dependent scattering theory for particles of finite charge.[43,44] The ground-state energy shift $\Delta E_K(y)$ is derived as a function of the reduced distance $y\equiv|\vec{\mathbf{R}}|/a_{2K}$ between the target nucleus and the point charge in first-order bound-state perturbation theory, i.e., to order Z_1/Z_2. In the present context, one can approximate the time-dependent $|\vec{\mathbf{R}}|$ by the particle impact parameter for reasons given in Appendix A. The average change in the binding energy $\hbar\langle\Delta\omega_{2K}\rangle$ is calculated by weighing the contribution for each impact parameter by the K-shell ionization probability function $|M_K(y/\xi_K)|^2$ and integrating over all impact parameters,

$$\hbar\langle\Delta\omega_{2K}(\xi_K)\rangle=\frac{\int_0^\infty \Delta E_K(y)|M_K(y/\xi_K)|^2\,y\,dy}{\int_0^\infty |M_K(y/\xi_K)|^2\,y\,dy}\ . \tag{35}$$

TABLE VI. Values of $g(\xi_K)$, where $\xi_K \equiv 2\eta_K^{1/2}/\theta_K$, for computing the binding factor $\epsilon = 1 + 2(Z_1/Z_{2K}\theta_K)\, g(\xi_K)$, Eq. (37). An approximate formula is given in Eq. (39).

ξ_K	η_K/θ_K^2	$g(\xi_K)$	ξ_K	η_K/θ_K^2	$g(\xi_K)$
0.0	0.0	1.000	1.6	0.64	0.429
0.04	0.0004	0.996	1.8	0.81	0.395
0.08	0.0016	0.985	2.0	1.00	0.366
0.16	0.0064	0.953	2.2	1.21	0.341
0.24	0.0144	0.912	2.4	1.44	0.319
0.32	0.0256	0.869	2.6	1.69	0.299
0.4	0.0400	0.826	2.8	1.96	0.282
0.48	0.0576	0.784	3.0	2.25	0.266
0.56	0.0784	0.745	3.4	2.89	0.240
0.64	0.1024	0.709	3.8	3.61	0.218
0.72	0.1296	0.674	4.2	4.41	0.200
0.8	0.1600	0.643	4.6	5.29	0.185
0.88	0.1936	0.614	5.0	6.25	0.171
0.96	0.2304	0.587	6.0	9.00	0.145
1.0	0.25	0.574	7.0	12.25	0.126
1.2	0.36	0.517	8.0	16.00	0.111
1.4	0.49	0.469	9.0	20.25	0.100

The velocity-dependent function $|M_K|^2$ derived by Bang and Hansteen[1] is proportional to $y^4 K_2^2(y/\xi_K)$, where K_2 is a modified Bessel function. The binding factor

$$\epsilon_K(\xi_K) = 1 + \langle \Delta\omega_{2K}(\xi_K)\rangle/\omega_{2K} \tag{36}$$

changes the target constant θ_K into a velocity-dependent function $\epsilon\theta_K$ which can be written[15]

$$\epsilon\theta_K \equiv \epsilon_K(\xi_K)\theta_K = [1 + 2(Z_1/Z_{2K}\theta_K)\, g(\xi_K)]\theta_K . \tag{37}$$

Appendix A gives details of this derivation. Values of $g(\xi_K)$ obtained by the numerical integration of Eq. (36) are listed in Table VI. It is monotonic with the limiting behavior

$$g(\xi_K) = \begin{cases} 1 - O(\xi_K^2) & \text{for } \xi_K \ll 1 \\ 0.95\xi_K^{-1} & \text{for } \xi_K \gg 1. \end{cases} \tag{38}$$

It can be calculated, with errors < 1%, from the formula

$$g(\xi_K) = (1+\xi_K)^{-5}(1 + 5\xi_K + 7.14\xi_K^2 + 4.27\xi_K^3 + 0.947\xi_K^4). \tag{39}$$

At high particle velocities, $\xi_K \gg 1$, the binding effects vanish as given in Eq. (38), which is consistent with Eq. (22). When $\xi_K \ll 1$, the influence of the binding effect, although due only to a small perturbation $(\epsilon - 1) \lesssim 2Z_1/Z_{2K}\theta_K$, can become large because $\sigma_K \propto (\epsilon\theta_K)^{-9}$ [Eq. (34)]. The function ϵ introduces additional dependences on $Z_1/Z_2\theta_K$ and ξ_K into the cross sections. When the binding effect is included, the cross section becomes

$$\sigma_K^B \equiv \sigma_K^{\mathrm{PWBA}}(\eta_K; \epsilon\theta_K) = (\sigma_{0K}/\epsilon\theta_K)\, F(\eta_K/(\epsilon\theta_K)^2), \tag{40}$$

where B denotes that the binding effect is included. The cross section is calculated by setting $y = \eta_K/(\epsilon\theta_K)^2$ and multiplying $F(y)$, Table V, by $\sigma_{0K}/\epsilon\theta_K$.

In summary of Secs. V A and V B, the formulas

$$\sigma_K = 9E_{10}(\pi d q_0 \epsilon)\, \sigma_K^{\mathrm{PWBA}}(\eta_K; \epsilon\theta_K) \tag{41}$$

$$= 9E_{10}(\pi d q_0 \epsilon)\left(\frac{\sigma_{0K}}{\epsilon\theta_K}\right) F\left(\frac{\eta_K}{(\epsilon\theta_K)^2}\right) \tag{42}$$

incorporate in an approximate but comprehensive manner the particle Coulomb deflection through $9E_{10}(\pi d q_0 \epsilon)$ and the change in K-shell binding through ϵ. The Coulomb deflection factor includes ϵ since $q_0 \propto \theta_K$. The same factors can be applied to the binary-encounter theory.

We note in conclusion that if one inserts $\epsilon\theta_K$ into Eq. (34), the total cross section Eq. (41) can be expanded in the limit $Z_1 e \to 0$ as

$$\sigma_K = \sigma_K^{\mathrm{PWBA}}[1 - \tfrac{9}{8}\pi q_0 d - 18(Z_1/Z_2\theta_K)\, g(\xi_K) + O(Z_1^2)]$$

$$= Z_1^2 F_2 - Z_1^3 F_3^g - Z_1^3 F_3^h + O(Z_1^4). \tag{43}$$

In this sense, the Coulomb deflection and the binding contribute terms which correspond, respectively, to the terms with coefficients J_{12} and J_{03} in the second plane-wave Born approximation, Eq. (14). Since F_3^g and F_3^h are positive they constitute *low-velocity subtractive "Z_1^3 effects."* High-velocity additive Z_1^3 effects have been identified recently.[12,13,15] They will be discussed in Paper II.

VI. UNIVERSAL CROSS SECTIONS

The impact of Coulomb deflection and of binding on the understanding of the experimental data is apparent in Fig. 7 if taken in juxtaposition with Fig. 5. The scaling proceeds in accordance with Eq. (42). The Coulomb deflection factor $9E_{10}(\pi d q_0 \epsilon)$ breaks the universal scaling rules through its dependence on the particle charge and mass, and therefore is divided out of the experimental cross sections σ_K^{expt}. The binding effect is taken into account by replacing θ_K with $\epsilon\theta_K$, Eq. (37), wherever θ_K appears in the scaling scheme suggested by the PWBA.

The low-velocity cross-section data in Fig. 7 cover six orders of magnitude as $\eta_K/(\epsilon\theta_K)^2$ changes by three orders of magnitude. For $\eta_K/(\epsilon\theta_K)^2 \lesssim 5 \times 10^{-2}$ the data unify to form one curve. The scatter in this domain is unsystematic and comparable to the experimental uncertainties.

When $5\times10^{-2} < \eta_K/(\epsilon\theta_K)^2 \lesssim 1$ the experimental points in Fig. 7 begin to spread significantly and rise above the theoretical curve. Such deviations from

the curve including the binding effects were reported earlier[12,13] and are apparent in the ratio curve Fig. 6. This new effect is indicative of the high-velocity additive Z_1^3 effect to be treated in Paper II.

The solid curve in Fig. 7 depicts the reduced theoretical cross section $\sigma_K^{\mathrm{PWBA}}(\eta_K;\epsilon\theta_K)/(\sigma_{0K}/\epsilon\theta_K) = F(\eta_K/(\epsilon\theta_K)^2)$ as listed in Table V. Although calculated from PWBA values for protons on aluminum,[36] Table V applies to all target elements with nonrelativistic K shells by virtue of Eq. (27). The order-of-magnitude discrepancies in Fig. 5 have been resolved in the frame of reference of Fig. 7.

The accuracy of the data and variations in the data analysis adopted in different laboratories limit the precision of the comparisons made in Fig. 7, and the problem of the proper choice of fluorescence yield is ever present. However, one can now deduce a consistent set of best fluorescence yields on the basis of observations with different particles at different velocities by normalizing the reduced x-ray cross sections to the PWBA curve in Fig. 7. This suggests, for example, that $\gamma_K(\mathrm{Al}) \simeq 4\times10^{-2}$ is a better value than the value[5] 3×10^{-2} chosen in preparing Fig. 7. Appendix B provides a sample calculation of a K-shell ionization cross section derived from the theory presented in this paper.

VII. SUMMARY

The analysis of new and existing data leads to an understanding of the observed behavior of cross sections for K-shell ionization under bombardment by various low-velocity heavy charged particles. One finds that the Coulomb deflection of the particles by the target nucleus and the perturbation of the initial atomic states by the incoming particle

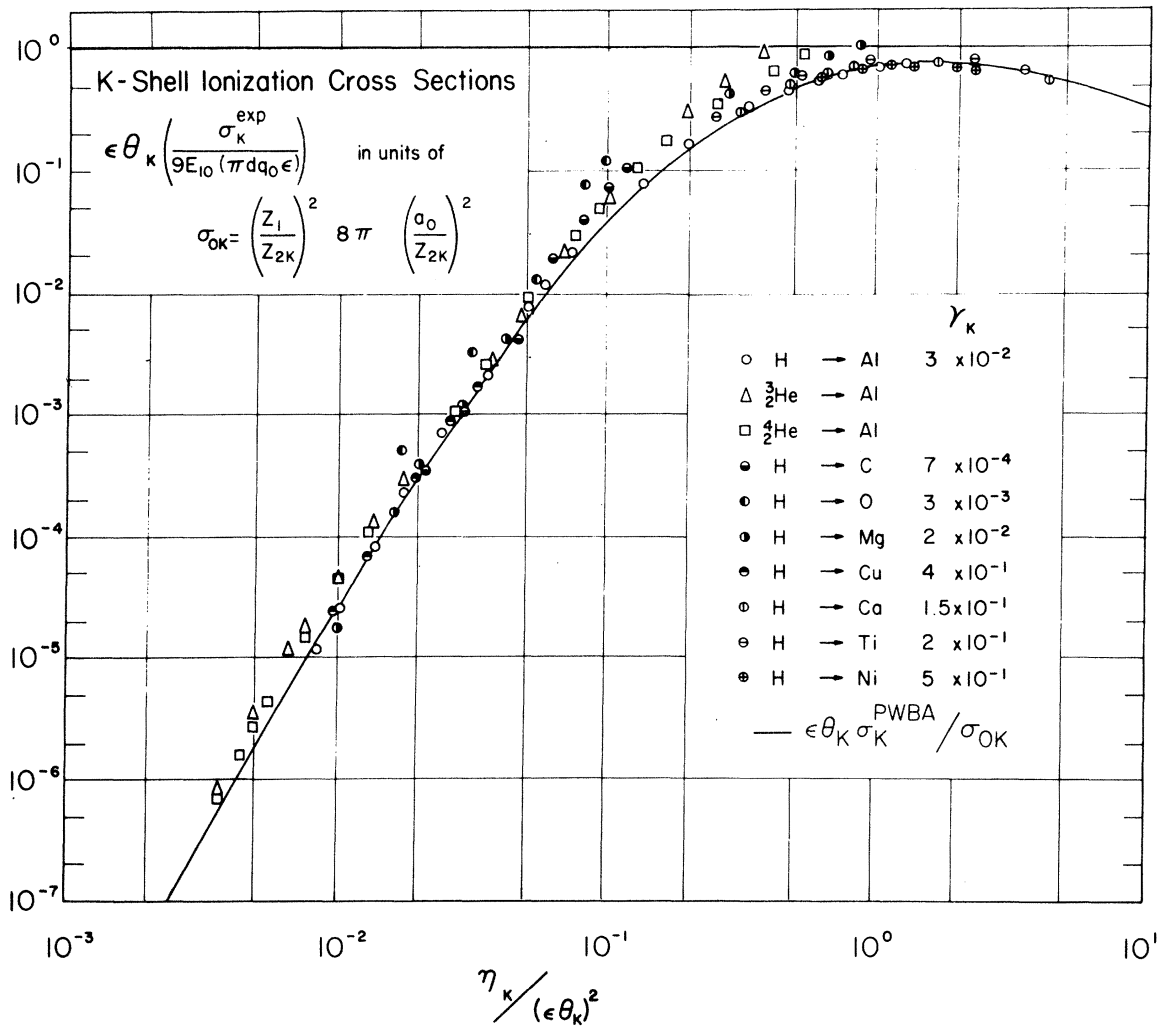

FIG. 7. Universal graph of K-shell ionization cross sections as prescribed by Eq. (42). The data are taken from Fig. 5 and Ref. 11. The curve is the PWBA prediction (Table V). The deviations when $0.05 < \eta_K/\epsilon^2\theta_K^2 < 1$ can be accounted for by incorporating the high-velocity Z_1^3 effect (Refs. 12 and 13) as reported in Paper II.

reduce the cross sections drastically. When these effects are incorporated into the theory, all known experimental cross sections exhibit a universal behavior. A unified experimental curve emerges which, in effect, represents an extrapolation of the data to the limiting conditions of zero projectile charge. This curve coincides with the predictions of the PWBA. The initial discrepancies of nearly two orders of magnitude are resolved. Agreement between experiment and the theory as developed here is now close to being limited by current experimental uncertainties.

ACKNOWLEDGMENTS

Many friends and colleagues have contributed through discussions and queries, and we are grateful to them. We thank Shirley A. McArthur for her help with the manuscript. The clarifying suggestions of Kenneth Stanton were legion and much appreciated. Our special gratitude goes to Arthur Schwarzschild for the stimulus and support he has given us over the years. We are indebted to Heinz-Dieter Carstanjen for assistance and to Louis Brown and his colleagues at the Carnegie Institution of Washington for the use of the accelerator.

APPENDIX A: DEVELOPMENT OF THE BINDING FACTOR

The semiclassical treatment of the K-shell ionization problem in first-order perturbation theory[1] gives the leading term of the low-velocity expansion of the differential probability for K-shell ionization to a final state of energy E_f as [cf. Eq. (3.12), Ref. 1]

$$|M_K(bq)|^2 \equiv \left(\frac{d\sigma_K}{dE_f}\right)_b = \frac{C}{2\pi} q^{-8}(bq)^4 K_2^2(bq), \tag{A1}$$

where C is a constant, $q = (\hbar\omega_{2K} + E_f)/\hbar v_1$, $K_2(bq)$ is a modified Bessel function, and b is the impact parameter. $M_K(y/\xi_K)$ is used in Eq. (35).

The total cross section is

$$\sigma_K(q_0) = \int_0^\infty dE_f \left[2\pi \int_0^\infty \left(\frac{d\sigma_K}{dE_f}\right)_b b\, db\right]$$

$$= 2\pi \int_0^\infty b\, db \left[\hbar v_1 \int_{q_0}^\infty \left(\frac{d\sigma_K}{dE_f}\right)_b dq\right], \tag{A2}$$

with $q_0 \equiv \omega_{2K}/v_1$.

The change in the binding energy $\Delta E_K(y)$ is given by first-order bound-state perturbation theory as

$$\Delta E_K(y) = \int \Psi_K^*(\vec{r})\ [Z_1 e^2/|\vec{R} - \vec{r}|]\Psi_K(\vec{r})\, d\vec{r}$$

$$= 2(Z_1/Z_{2K})Z_{2K}^2 (\mathrm{Ry})\, y^{-1}[1 - (1+y)e^{-2y}], \tag{A3}$$

with the notation $y = |\vec{R}|/a_{2K}$. $\vec{R}$ is the particle coordinate for a straight-line trajectory, $\vec{r}$ is the electron coordinate, and $\Psi_K(\vec{r})$ is the unperturbed nonrelativistic hydrogenic K-shell wave function. The particle excites the K-shell electrons while moving with velocity $v_1 < v_{2K}$ at the distance $|\vec{R}| = (b^2 + v_1^2 t^2)^{1/2}$. Hence $\Delta E_K(y)$ varies with time. In practice, the binding effect is incorporated by adding $\Delta E_K(y)$ to $\hbar\omega_{2K}$ in the integration over time which leads to Eq. (A1). We make use of the fact that the principal contribution to the time integration comes from the interval $|t| \lesssim (q_0 v_1)^{-1} = \omega_{2K}^{-1}$. This limits the range of $|\vec{R}|$ in the time integration for fixed impact parameter to $b \leq |\vec{R}| \lesssim (b^2 + q_0^{-2})^{1/2}$. Since the largest contribution to the impact parameter integration, Eq. (A2), comes from values $b \approx q_0^{-1}$, $|\vec{R}|$ varies between b and $\sqrt{2}\,b$ in the time integration at impact parameters of importance. At $b = q_0^{-1}$, for example, $\xi_K \leq y \lesssim \sqrt{2}\,\xi_K$ in the time integration. Thus, at low velocities, $y \ll 1$. Since $\Delta E_K(y)$ is a slowly varying function for $y \ll 1$, omitting the time dependence of y for the sake of convenience should not cause significant error. This is illustrated by replacing ξ_K by $\sqrt{2}\,\xi_K$ (corresponding to the upper limit of y) in the function $g(\xi_K)$ (cf. Table VI). The shift $\epsilon - 1$ from Eq. (37) diminishes by at most 15% in its range of validity $\xi_K < 1$. Thus in what follows we set $y = b/a_{2K}$.

The binding effect is incorporated into Eq. (A2) by adding $\Delta E_K(y)$ to $\hbar\omega_{2K}$ or, equivalently, $\Delta q(y) \equiv \Delta E_K(y)/\hbar v_1$ to q_0. This gives

$$\sigma_K^B = C\hbar v_1 \int_0^\infty b^5\, db \int_{q_0 + \Delta q(y)}^\infty q^{-4} K_2^2(bq)\, dq$$

$$= C\hbar v_1 \int_0^\infty b^8\, db D(bq_0 + b\Delta q(y)), \tag{A4}$$

where the superscript B denotes the binding effect and

$$D(z) \equiv \int_z^\infty u^{-4} K_2^2(u)\, du. \tag{A5}$$

The use of first-order perturbation theory for the binding effect suggests that $D(bq_0 + b\Delta q(y))$ be expanded in a Taylor series to order $\Delta q(y) \propto (Z_1/Z_{2K})$,

$$D(bq_0 + b\Delta q(y)) = D(bq_0) - (bq_0)^{-4} K_2^2(bq_0) b\Delta q(y) + O(\Delta q(y)^2). \tag{A6}$$

Thus

$$\sigma_K^B \simeq C\hbar v_1 [q_0^{-9} \int_0^\infty x^8 D(x)\, dx - q_0^{-10} \int_0^\infty \Delta q(x\xi_K)\, x^5 K_2^2(x)\, dx], \tag{A7}$$

where $x = bq_0$ and $\int_0^\infty x^8 D(x)\, dx = \frac{1}{9}(2^2/5)$. The binding effect may be identified as a Z_1^3 term by noting that $C \propto Z_1^2$ and $\Delta q(y) \propto Z_1$ [cf. Eq. (A3)]. Then Eq. (A7) can be written

$$\sigma_K^B \simeq \sigma_K^{\mathrm{PWBA}}(q_0)[1 - 9q_0^{-1}(5/2^5) \int_0^\infty \Delta q(x\xi_K)\, x^5 K_2^2(x)\, dx], \tag{A8}$$

where

$$\sigma_K^{\mathrm{PWBA}}(q_0) = \tfrac{1}{9}\, C\hbar v_1 (2^5/5) q_0^{-9}, \tag{A9}$$

which is equivalent to Eq. (34).

It is convenient to employ the approximation

$$1 - 9q_0^{-1}(5/2^5)\int_0^\infty \Delta q(x\xi_K)\,x^5K_2^2(x)\,dx$$

$$\simeq [1+q_0^{-1}(5/2^5)\int_0^\infty \Delta q(x\xi_K)\,x^5K_2^2(x)\,dx]^{-9}, \quad \text{(A10)}$$

because it reestablishes the binding effect as a shift of order Z_1/Z_{2K} in the binding energy, rather than a subtractive term of order $(Z_1/Z_{2K})^3$ to the cross section. This device also provides a succinct way of incorporating the binding effect into the cross section to all orders in v_1. By defining ϵ, Eq. (37), as

$$\epsilon \equiv 1+q_0^{-1}(5/2^5)\int_0^\infty \Delta q(x\xi_K)\,x^5K_2^2(x)\,dx, \quad \text{(A11)}$$

we note, from Eqs. (A8) and (A9), that

$$\sigma_K^B \simeq \sigma_K^{\mathrm{PWBA}}(q_0)\epsilon^{-9} = \sigma_K^{\mathrm{PWBA}}(q_0\epsilon) = \sigma_K^{\mathrm{PWBA}}(\epsilon\omega_{2K}/v_1). \quad \text{(A12)}$$

Since $y = x\xi_K$ and $\hbar v_1 \Delta q(x\xi_K) = \Delta E_K(y)$, we identify Eq. (A11) with Eq. (36) and retrieve Eq. (35) in the form

$$\hbar\langle\Delta\omega_{2K}(\xi_K)\rangle = \hbar\omega_{2K}q_0^{-1}(5/2^5)\int_0^\infty \Delta q(x\xi_K)\,x^5K_2^2(x)\,dx. \quad \text{(A13)}$$

Equation (40) then follows from Eq. (A12). This step introduces the function ϵ into the calculation of the universal cross section σ_K^B.

APPENDIX B: SAMPLE CALCULATION OF K-SHELL IONIZATION CROSS SECTION

To find the cross section for 408-keV helium ($Z_1 = 2$, $M_1 = 4$ amu) on aluminum ($Z_2 = 13$, $M_2 = 27$ amu, $\hbar\omega_{2K} = 1559.6$ eV), values for the binding factor ϵ, and the Coulomb deflection factor $9E_{10}(\pi dq_0\epsilon)$ must be computed. With

$$\theta_K = \hbar\omega_{2K}/Z_{2K}^2\mathcal{R} = 1560\ \text{eV}/(13-0.3)^2\times 13.6\ \text{eV}$$

$$= 0.711$$

and

$$\eta_K = \left(\frac{v_1}{v_{2K}}\right)^2 = \frac{\frac{1}{2}M_1v_1^2}{Z_{2K}^2\mathcal{R}\,M_1/m_e}$$

$$= 408\ \text{keV}/(12.7)^2(13.6\ \text{eV}\times 1836\times 4) = 0.0253,$$

one finds $\eta_K/\theta_K^2 = 0.0501$. From Table VI or Eq. (39) one obtains $g(\xi_K) = 0.800$. Then ϵ is calculated as follows:

$$\epsilon = 1 + 2\frac{Z_1}{Z_{2K}}\theta_K^{-1}\,g(\xi_K) = 1 + 2\,\frac{2}{12.7}\,\frac{0.800}{0.711}$$

or $\epsilon = 1.355$. This gives $\epsilon\theta_K = 0.963$ and $\eta_K/(\epsilon\theta_K)^2 = 0.0273$. The value of $F(y) = \sigma_K^B(\sigma_{0K}/\epsilon\theta_K)^{-1}$ for $y = \eta_K/(\epsilon\theta_K)^2 = 0.0273$, obtained by interpolation from Table V, is 8.12×10^{-4}. Since

$$\sigma_{0K} = (Z_1/Z_{2K})^2\,8\pi a_{2K}^2 = (Z_1/Z_{2K}^2)^2\,8\pi a_0^2$$

$$= [2/(12.7)^2]^2\ 7.04\times 10^{-16}\ \text{cm}^2$$

$$= 1.08\times 10^{-19}\ \text{cm}^2,$$

we obtain

$$\sigma_K^B = 8.12\times 10^{-4}\times 1.08\times 10^{-19}\ \text{cm}^2/0.963$$

$$= 9.12\times 10^{-23}\ \text{cm}^2.$$

This is the theoretical K-shell ionization cross section which includes the binding effect. To find the Coulomb deflection factor, the value of

$$dq_0 = \tfrac{1}{2}Z_1\theta_K(m_e/M)/\eta_K^{3/2}$$

must be calculated, where $M = M_1M_2/(M_1+M_2)$ is the reduced mass:

$$M = 4\times 27/(4+27) = 3.48\ \text{amu},$$

$$dq_0 = \tfrac{1}{2}(2)(0.711)/(1836\times 3.48\times 0.00403) = 0.0276.$$

The argument of the Coulomb deflection factor becomes

$$\pi dq_0\epsilon = 3.14\times 0.0276\times 1.355 = 0.117$$

so that[42]

$$9E_{10}(0.117) = 9\times 0.0974 = 0.876.$$

Thus the theoretical prediction of the K-shell ionization cross section, including the Coulomb deflection and binding effects, becomes

$$\sigma_K = 9E_{10}(\pi dq_0\epsilon)\,\sigma_K^B = 0.876\times 9.12\times 10^{-23}\ \text{cm}^2$$

$$= 8.00\times 10^{-23}\ \text{cm}^2 = 80\ \text{b}.$$

Comparison with the experimental x-ray cross section from Table IV, $\sigma_x(408\ \text{keV}) = (3.25\pm 0.8)$ b gives, for this example, the fluorescence yield

$$\gamma_K(\text{Al}) = (\sigma_x/\sigma_K) = 4.1\times 10^{-2}\pm 25\%,$$

which is somewhat higher than the mean value 3×10^{-2} used in Figs. 5 and 7.

Because of Eq. (27), the values given in Table V, although calculated for aluminum, can be used for any target as long as $\eta_K/(\epsilon\theta_K)^2 \leq 10$. For high velocities, more accurate cross sections for other targets can be obtained by recourse to the source[36] of the universal function given in Table V.

---

*Work supported by the U.S. Atomic Energy Commission.

†Also Finch College, New York, N. Y. 10021.

[1]J. Bang and J. M. Hansteen, K. Dan. Vidensk. Selsk. Mat.-Fys. Medd. 31, No. 13 (1959).

[2]J. Chadwick, Philos. Mag. **24**, 594 (1912).

[3]C. Gerthsen, Z. Phys. **36**, 540 (1926).

[4]Cf. E. Merzbacher and H. W. Lewis, in *Handbuch der Physik*, edited by S. Flügge (Springer-Verlag, Berlin, 1958), Vol. 34, p. 166 ff., and references cited therein.

[5]J. M. Khan and D. L. Potter, Phys. Rev. 133, A890 (1964); J. M. Khan, D. L. Potter, and R. D. Worley, Phys. Rev. 139, A1735 (1965).

[6]W. Brandt, R. Laubert, and I. Sellin, Phys. Lett. **21,** 518 (1966).
[7]W. Brandt, R. Laubert, and I. Sellin, Phys. Rev. **151,** 56 (1966).
[8]W. Brandt and R. Laubert, Phys. Rev. **178,** 225 (1969).
[9]R. R. Hart, F. W. Reuter, H. P. Smith, and J. M. Khan, Phys. Rev. **179,** 4 (1969).
[10]W. Brandt and R. Laubert, Phys. Rev. Lett. **24,** 1037 (1970).
[11]G. A. Bissinger, J. M. Joyce, E. J. Ludwig, W. McEver, and S. M. Shafroth, Phys. Rev. A **1,** 841 (1970).
[12]G. Basbas, W. Brandt, and R. Laubert, Phys. Lett. **34A,** 277 (1971).
[13]G. Basbas, W. Brandt, R. Laubert, A. Ratkowski, and A. Schwarzschild, Phys. Rev. Lett. **27,** 171 (1971).
[14]J. D. Garcia, Phys. Rev. A **1,** 280 (1970); Phys. Rev. A **1,** 1402 (1970); Phys. Rev. A **4,** 955 (1971).
[15]W. Brandt, in *Proceedings of the International Conference on Inner-Shell Ionization Phenomena and Future Applications, Atlanta, Georgia,* 1972, edited by R. W. Fink, S. T. Manson, J. M. Palms, and P. V. Rao (U.S. AEC, Oak Ridge, Tenn., 1973), p. 948ff
[16]R. Laubert and N. Wotherspoon, IEEE Trans. Nucl. Sci. **12,** 285 (1965).
[17]The isotropy of x-ray emission has been shown experimentally for Au(L) x rays [E. M. Bernstein and H. W. Lewis, Phys. Rev. **95,** 83 (1954)] and for Ti(K) and Sn(K) x rays [C. W. Lewis, R. L. Watson, and J. B. Natowitz, Phys. Rev. A **5,** 1773 (1972)].
[18]A minimization procedure based on the variable-metric technique employed by R. Fletcher and M. J. D. Powell [Comput. J. **6,** 163 (1963)] was used to fit analytical functions to the yield data.
[19]C. Varelas and J. Biersack, Nucl. Instrum. Methods **79,** 213 (1970).
[20]J. Lindhard, M. Scharff, and H. E. Schiøtt, K. Dan. Vidensk. Selsk. Mat.-Fys. Medd. **34,** No. 14 (1965).
[21]W. White and R. M. Mueller, J. Appl. Phys. **30,** 3660 (1967).
[22]J. D. Moorhead, J. Appl. Phys. **36,** 394 (1965).
[23]W. Whaling, in *Handbuch der Physik*, edited by S. Flügge (Springer-Verlag, Berlin, 1958), Vol. 34, p. 193ff.
[24]D. I. Porat and K. Ramavataram, Proc. Phys. Soc. Lond. 78, 1135 (1961).
[25]S. K. Allison and D. Warshaw, Rev. Mod. Phys. **25,** 779 (1953).
[26]J. H. Ormrod, J. R. MacDonald, and H. E. Duckworth, Can. J. Phys. **43,** 275 (1965).
[27]L. P. Nielsen, K. Dan. Vidensk. Selsk. Mat.-Fys. Medd. 33, No. 6 (1961).
[28]W. K. Chu and D. Powers, Phys. Rev. **187,** 478 (1969).
[29]A. J. Bearden, J. Appl. Phys. **37,** 1681 (1966).
[30]P. B. Needham, Jr. and B. D. Sartwell, Phys. Rev. A **2,** 27 (1970).
[31]K. Shima, I. Makino, and M. Sakisaka, J. Phys. Soc. Jap. **30,** 611 (1971).
[32]The formal basis for developing a Born series for such a Hamiltonian can be found in the book by M. L. Goldberger and K. M. Watson [*Collision Theory* (Wiley, New York, 1964), p. 202ff].
[33]W. Kohn, Rev. Mod. Phys. **26,** 292 (1954).
[34]E. J. Williams, Rev. Mod. Phys. **17,** 217 (1945).
[35]G. Basbas and G. S. Khandelwal, Bull. Am. Phys. Soc. **11,** 307 (1966).
[36]G. S. Khandelwal, B. H. Choi, and E. Merzbacher, At. Data **1,** 103 (1969).
[37]F. Herman and S. Skillman, *Atomic Structure Calculations* (Prentice-Hall, Englewood Cliffs, N. J., 1963).
[38]G. S. Khandelwal, Phys. Rev. **167,** 136 (1968).
[39]G. Basbas, Bull. Am. Phys. Soc. **14,** 631 (1969); Bull. Am. Phys. Soc. **16,** 564 (1971).
[40]R. Fink, R. C. Jopson, H. Mark, and C. R. Swift, Rev. Mod. Phys. **83,** 513 (1966).
[41]T. Huus, J. H. Bjerregaard, and B. Elbek, K. Dan. Vidensk. Selsk. Mat.-Fys. Medd. **30,** No. 13 (1956).
[42]*Handbook of Mathematical Functions,* edited by M. Abramowitz and I. A. Stegun (Dover, New York, 1965). The approximation $9E_{10}(x)=[9/(9+x)]\ e^{-x}$ is adequate for our purposes.
[43]N. F. Mott, Proc. Camb. Philos. Soc. **27,** 533 (1931).
[44]G. Basbas, W. Brandt, and R. H. Ritchie, Phys. Rev. A (to be published).

PHYSICAL REVIEW A VOLUME 7, NUMBER 3 MARCH 1973

Total Gamma-Ray Cross Sections in the Energy Region 60–1400 keV

K. Sivasankara Rao, B. V. Thirumala Rao, B. Mallikarjuna Rao, V. Visweswara Rao,* and K. Parthasaradhi
The Laboratories for Nuclear Research, Andhra University, Visakhapatnam, India
(Received 18 August 1972)

Total γ-ray cross sections at 12 γ energies (most of them are at new energies) are determined in Cu, W, and Pb and the results are reported. The error in these results is of the order of 1%. An analysis of the data is presented.

I. INTRODUCTION

In previous investigations,[1,2] it was shown that there are inconsistencies in the available total γ-ray experimental cross sections. Recently a few measurements were reported.[3,4] However, there remain large energy gaps, especially above 145 keV. Hence, in the present investigations these cross sections are measured at 12 γ energies (most of them are at new energies) in a wide energy region from 60 to 1400 keV in three typical elements, viz., Cu, W, and Pb, and the results are reported.

II. EXPERIMENTAL DETAILS AND RESULTS

The total γ-ray cross sections can be measured by conducting the usual transmission experiment[3–6] on a good geometry setup. A similar[3–6] good